D0 note 5527 v0.3

Measurement of the $t\bar{t}$ Production Cross-Section at $\sqrt{s} = 1.96$ TeV in the Lepton+Jets Final State using kinematic information on 1 fb^{-1} of DØ Data

DooKee Cho[1], Ulrich Heintz[1], Meenakshi Narain[2], Marc-André Pleier[3], Michele Weber[4], Hwidong Yoo[2]

[1]Boston University, Boston, MA, USA
[2]Brown University, Providence, RI, USA
[3]Universität Bonn, Bonn, Germany
[4]Universität Bern, Bern, Switzerland
(Dated: November 9, 2007)

A measurement of the $t\bar{t}$ production cross-section at $\sqrt{s} = 1.96$ TeV, based on the application of likelihood discriminant to data preselected in the l+jets channel (e+jets: 912.5) pb^{-1}, μ+jets: 871.3 pb^{-1}) is presented. The cross-section is:

$$e + \text{jets} \ : \quad \sigma_{p\overline{p}\to t\overline{t}+X} = 6.22^{+1.04}_{-1.00}\ (\text{stat})\ ^{+0.52}_{-0.40}\ (\text{syst})\ \pm 0.38\ (\mathcal{L})\ \text{pb}$$

$$\mu + \text{jets} \ : \quad \sigma_{p\overline{p}\to t\overline{t}+X} = 7.06^{+1.21}_{-1.17}\ (\text{stat})\ ^{+0.84}_{-0.57}\ (\text{syst})\ \pm 0.43\ (\mathcal{L})\ \text{pb}$$

$$l + \text{jets} \ : \quad \sigma_{p\overline{p}\to t\overline{t}+X} = 6.59^{+0.78}_{-0.77}\ (\text{stat})\ ^{+0.60}_{-0.37}\ (\text{syst})\ \pm 0.40\ (\mathcal{L})\ \text{pb}$$

Contents

I. INTRODUCTION

In $p\bar{p}$ collisions at Tevatron energy the Standard Model (SM) top quark is expected to be dominantly produced in pairs via the strong interaction ($q\bar{q}$ annihilation (85%) and gluon fusion (15%)) [1, 2]. The top quark decays subsequently to a W boson and a b quark nearly 100% of the time. The final states which are visible in the detector are fully determined by the decay modes of the two W bosons. In this analysis the combination of one W decaying to leptons (e or μ in this analysis) and one to hadrons is considered. Therefore, the final states in this analysis consist of one isolated, high p_T lepton, missing transverse energy ($\not\!\!E_T$) from a neutrino, and associated jets.

The dominant physics background to such a signature arises from W boson production accompanied by four or more jets. Instrumental backgrounds for these channels originate primarily from multijet processes with jets faking leptons.

Signal-to-background discrimination can be achieved by making use of differences of kinematic information in the event or the rate at which at least one of the jets per event is identified as b-jet. This analysis evaluates the $t\bar{t}$ production cross section in the l+jets channel using kinematic information from the p17 data set of about 900 pb^{-1}. It is based on the preliminary result from fall 2006 [3].

II. OBJECT IDENTIFICATION

We define the following fundamental objects: primary vertex, leptons, jets and missing transverse energy $\not\!\!E_T$. These objects, their reconstruction and the respective selection criteria are described in [4–9].

A. Primary Vertices

The primary vertex (PV) defines the place of hard interaction in the detector and is the reference point for the calculation of kinematic variables, such as transverse momenta. Since p14 we have been using the Adaptive PV algorithm [10]. In order to ensure high quality of the reconstructed vertex while keeping the efficiency high, the following additional PV selection is required:

- $|z_{PV}| \leq 60$ cm (PV within the SMT fiducial region).
- At least three tracks fitted to the PV.

B. Electrons

Electrons are clusters of energy depositions in the electromagnetic section of the calorimeter consistent in shape with an electromagnetic shower. We accept electrons in the central calorimeter only ($|\eta| < 1.1$). At least 90% of their energy must be in the electromagnetic section of the calorimeter and the χ^2 from the 7×7 Hmatrix must be less than 50. The energy cluster must be isolated from other energy deposits in the calorimeter. The fraction of energy in an annular isolation cone of radius $0.2 < R < 0.4$, $R = \sqrt{\Delta\phi^2 + \Delta\eta^2}$ must be less than 15% of the energy in the core cone of radius $R < 0.2$. Every electron must be matched to a charged particle track from the tracking detectors with $p_T > 5$ GeV. In order to be counted as tight electrons, the candidates must also have an electron likelihood value[11] > 0.85. In this analysis we used the emid_cuts package version v02-04-08 (emid_cuts/support/emid_cuts.txt). We used version 3 top_loose for loose electrons and version 3 top_tight for tight electrons.

C. Muons

Muons are reconstructed primarily as tracks in the muon spectrometer. We accept muons with $|\eta| < 2$ and they must be of "medium NSeg3" quality. We apply the standard loose cosmic ray rejection selection requiring A and BC scintillator times $|t| < 10$ ns. The track reconstructed in the muon system must match a track reconstructed in the central tracker with $\chi^2/\mathrm{ndf} < 4$. In p17 muon ID doesn't use dca significance cut any more. It uses $|dca(x, y)| < 0.2$ for tracks without SMT hits and $|dca(x, y)| < 0.02$ for tracks with SMT hits. Muons must be separated from jets by $\Delta R = \sqrt{\Delta\eta^2 + \Delta\phi^2} > 0.5$. Muons are counted as tight if the energy deposited in an annular cone of radius $0.1 < R < 0.4$ around the muon direction is less than 8% of the muon p_T and if the momenta of all tracks in a cone of radius $R < 0.5$ around the muon direction, except the track matched to the muon, add up to less than 6% of the muon p_T.[12]

D. Jets

Before jet reconstruction the T42 algorithm [13] is run to remove isolated small energy deposits that are likely due to noise. Jets are reconstructed from energy deposits in the calorimeter using the Run 2 cone algorithm [14]. Jets with $p_T > 15$ GeV are accepted within $|\eta| < 3.4$. (The jet E_T cut is made after all corrections have been applied.) The jet quality cuts have been divided up as a function of the η^{det} region of the calorimeter in p17, which was not done in p14. The cuts include requirements on the coarse hardronic fraction of the energy, the electromagnetic fraction, and a trigger level 1 ratio requirement, and are listed on p.20 of [7].

Preliminary p17 jet energy scale corrections are applied to jets in the data to convert jet energies from d0reco to particle-level energies [15]. Additionally, jets containing a muon within $\Delta R(\mu, jetaxis) < 0.5$ are considered to originate from a semileptonic b-quark decay and are corrected for the momentum carried away by the muon and the neutrino. For this correction, it is assummed that the neutrino carries the same momentum as the muon.

Monte Carlo jets need to be corrected for differences in the reconstruction and identification efficiency, for the worse energy resolution in the data than in the simulation, and for different calorimeter responses. The standard Jet Energy Scale Group's "jet shifting, smearing, and removal algorithm"(JSSR) [16] is applied with p17-derived smearing resolutions, and removal of $p_T < 15$ GeV jets, but no shifting to correct for the mean transvers energy imbalance.

E. Missing Transverse Momentum

Neutrinos carry away momentum that can be inferred using momentum conservation in the transverse plane. The sum of the transverse momenta of undetected neutrinos is equal to the negative sum of the transverse momenta of all particles that were observed in the detector. In practice we compute the missing transverse momentum by adding up vectorially the transverse energies in all cells of the electromagnetic and fine hadronic calorimeters. Cells in the coarse hadronic calorimeter are only added if they are part of a good jet. This raw quantity is then corrected for the energy corrections applied to the reconstructed objects and for the momentum of all muons in the event, corrected for their energy loss in the calorimeter. .

III. DATA SAMPLES AND MONTE CARLO SIMULATION

A. Data Sample

The data sample is derived from the CSG skims [17] collected between August 2002 and December 2005, with run numbers 151,817–213,063 and the selection criteria for data are described in [18]. We do not include in this analysis the ≈ 60 pb^{-1} of data taken in January and February 2006 when cables in the calorimeter readout were swapped. We use the top_cafe package for skimming and selection of these samples [19]. The triggers used for this analyses are described in [20]. A summary of trigger lists and luminosities can be found in Table 1 and 2. All the numbers are derived with the new luminosity constant and back propagation including radiation damage and single diffractive efficiency corrections [21, 22].

Trigger Version	Trigger Name	Delivered (pb^{-1})	Recorded (pb^{-1})	Good Quality (pb^{-1})
V8.0 - V9.0	EM15_2JT15	6.17	4.94	4.86
V9.0 - V10.0	EM15_2JT15	47.84	41.73	24.73
V10.0 - V11.0	EM15_2JT15	20.35	18.29	9.81
V11.0 - V12.0	EM15_2JT15	78.87	71.83	62.82
V12.0 - V13.0	E1_SHT15_2J20	272.64	250.76	227.14
V13.0 - V13.3	E1_SHT15_2J_J25	80.43	73.02	54.81
V13.3 - V14.0	E1_SHT15_2J_J30	353.70	324.69	294.27
V14.0 - V15.0	E1_SHT15_2J_J25	290.01	270.62	234.11
T O T A L		1150.01	1055.88	912.55

TABLE 1: New integrated luminosities by trigger list version for the e+jets channel.

Trigger Version	Trigger Name	Delivered (pb^{-1})	Recorded (pb^{-1})	Good Quality (pb^{-1})
V8.0 - V9.0	MU_JT20_L2M0	7.23	5.75	5.64
V9.0 - V10.0	MU_JT20_L2M0	47.89	41.77	24.77
V10.0 - V11.0	MU_JT20_L2M0	21.37	19.30	10.70
V11.0 - V12.0	MU_JT20_L2M0	79.27	74.34	65.24
V12.0 - V13.0	MU_JT25_L2M0	277.02	254.96	230.93
V13.0 - V13.2	MUJ2_JT25	55.74	39.47	31.43
V13.2 - V13.3	MUJ2_JT25_LM3	26.27	22.26	16.10
V13.3 - V14.0	MUJ2_JT30_LM3	382.01	277.12	252.17
V14.0 - V14.2	MUJ1_JT25_LM3	0.01	0.01	0.01
V14.2 - V14.3	MUJ1_JT25_ILM3	24.83	22.81	20.84
V14.3 - V15.0	MUJ1_JT35_LM3	265.45	248.06	213.51
T O T A L		1187.09	1005.85	871.34

TABLE 2: New integrated luminosities by trigger list version for the μ+jets channel.

B. Monte Carlo Simulation

In this analysis, we use $t\bar{t}$ MC samples generated with PYTHIA 6.323 [23]. The cross section measurement is based on $t\bar{t}$ samples, for which the top quark mass was set to 175 GeV and the factorization scale was set to $m_t^2 + \sum p_T^2$(jets). We also use $t\bar{t}$ MC samples with the top quark mass set to 165, 170, 180, 185, and 190 GeV to determine the mass dependence of the measured $t\bar{t}$ cross section. These were generated with PYTHIA in the same way as the main $t\bar{t}$ sample except for the top quark mass.

W+jets samples were generated using ALPGEN [24] with a jet-matching algorithm, following the MLM prescription [25]. The sample was broken down into three subsamples by parton flavors: Wbb, Wcc, Wjj + extra light partons. Here j stands for light quarks and gluons. The matching algorithm ensures that each jet is generated by ALPGEN at the parton level and not filled in by PYTHIA, thus avoiding double counting of events in certain regions of ΔR and p_{T} space for the radiated jets.The factorization scale was set to $m_W^2 + p_T^2(W)$.

We also simulated single top, $Z(\rightarrow$ ee, $\mu\mu$, $\tau\tau)$+jets and diboson production. The Z+jets process generated with ALPGEN was broken down into $Zb\bar{b}$, $Zc\bar{c}$ and $Zq\bar{q}$ + light parton samples in the same way as the W+jets samples.

Single top event samples were generated by the COMPHEP [27] Monte Carlo event generator with top quark mass set to 175 GeV. Diboson samples (WW, WZ and ZZ) were generated with PYTHIA.

The CTEQ6L1 pdf set [28] was used for all Monte Carlo samples.

For all the Monte Carlo event sets we removed duplicate events caused by a bug in the setting of the random number seeds, which were out of the allowed range. For the W+jets sets we have also removed events with heavy flavor jets added by PYTHIA so as not to duplicate the phase space of those already generated by ALPGEN [29]. The Wcj subprocesses were included in the Wjj sample with massless charm quarks.

We estimated the contribution from multijet events using the fake rates measured in a sample with **Loose** selection with $\not\!\!E_T < 10$ GeV [34]. For all control plots we use the events which pass the **Loose** selection (described in section V A) but not the **Tight** selection (**L-T** sample). The data and MC samples for this analysis are described in [30].

IV. THE $t\bar{t}$ EVENT SELECTION

A. Preselection

The signature of the lepton+jets channel is one isolated lepton with high transverse momentum, large $\not\!\!E_T$ due to the undetected neutrino and four or more jets with high transverse momentum, two of which are b-jets. The preselection is designed to define a data sample enriched in W+jets and top events. To ensure that the lepton+jets analyses are orthogonal to each other and to the dilepton analyses, events with a second lepton with high transverse momentum are explicitly vetoed.

To summarize, the following requirements are imposed to preselect the data sample for:

- Good quality [31]
- At least three jets with $p_T > 20$ GeV and $|\eta| < 2.5$, leading jet $p_T > 40$ GeV.
- Good vertex with $|z_{PV}| \leq 60$ cm with at least 3 tracks attached.
- $\sum$ Jet $p_T > 120$ GeV if there are only three jets in the event.

For the e+jets channel, we require additional selection as follows:

- One tight electron (as defined in section II B) with $p_T > 20$ GeV in the CC.
- No second tight electron with $p_T > 15$ GeV in CC or EC.
- No isolated muon with $p_T > 15$ GeV.
- Electron coming from the primary vertex: $|\Delta z(e, PV)| < 1$ cm.
- $\not\!\!E_T > 20$ GeV and $\Delta\phi(e, \not\!\!E_T) > 0.7 \cdot \pi - 0.045 \cdot \not\!\!E_T$.

For the μ+jets channel, we require addition selection as follows:

- One tight muon (as defined in section II C) with $p_T > 20$ GeV.
- Invariant mass of the selected muon and any second muon $m_{\mu\mu} < 70$ GeV or $m_{\mu\mu} > 110$ GeV to reject $Z(\rightarrow \mu\mu)$+jet events.
- No second muon with $p_T > 15$ GeV with muon quality MediumNSeg3.
- No tight electron with $p_T > 15$ GeV.
- Muon coming from the primary vertex: $|\Delta z(\mu, PV)| < 1$ cm.
- $\not\!\!E_T > 25$ GeV and $\Delta\phi(\mu, \not\!\!E_T) > 2.1 - 0.035 \cdot \not\!\!E_T$.

The main background source for $t\bar{t}$ apart from W+jets production are multijet events with a jet misidentified as a lepton or a lepton produced inside a jet. Thus multijet events contain both real and fake leptons. At the same time an energy imbalance in multijet events occurs predominantly due to jet energy mismeasurements, in which case the direction of the missing transverse energy points along (or opposite) one of the objects (lepton or jet) in the event. In order to suppress the multijet background more efficiently than just by selecting on missing transverse energy ($\not\!\!E_T$) alone, the different angular distributions between the missing transverse energy and the lepton can be exploited without suffering from a large efficiency loss.

Tables 3 through 6 show all selections in the order in which they are applied to the data set and the corresponding exclusive and cumulative efficiencies as found in the $t\bar{t}$ signal MC. There are separate tables for the third exclusive jet bin and the fourth inclusive jet bin. The total efficiency for the preselection for $t\bar{t}$ events ($\varepsilon_{preselection}$) is measured in the $t\bar{t}$ simulation with respect to $t\bar{t} \rightarrow \ell\nu_\ell q\bar{q}' b\bar{b}$, where ℓ can be an electron or muon from the decay of a W boson, including $W \rightarrow \tau\nu$ decays.

Lastly the data quality selection has to be considered. While the removal of whole runs or luminosity blocks can be taken into account in the luminosity calculation, the event based data quality had to be included in the preselection efficiency. This efficiency has been measured in [32] to be 97.14 % with an insignificant statistical error. This systematic error has been assigned in systematics for luminosity.

Selection or κ	Events left	Exclusive selection efficiency[%]	Cumulative selection efficiency[%]
	242352		
# good jets =3	92423	38.14 ± 0.10	38.14 ± 0.10
Leading jet > 40 GeV	91189	98.66 ± 0.04	37.63 ± 0.10
Loose electron	48421	53.10 ± 0.17	19.98 ± 0.08
Muon veto	48411	99.98 ± 0.01	19.98 ± 0.08
2nd electron veto	48401	99.98 ± 0.01	19.97 ± 0.08
Vertex selection	47693	98.54 ± 0.05	19.68 ± 0.08
$\not\!\!E_T$ > 20 GeV	42353	88.80 ± 0.14	17.48 ± 0.08
Triangle selection	39745	93.84 ± 0.11	16.40 ± 0.08
Tight electron	35156	88.45 ± 0.16	14.51 ± 0.07
Trigger probability		0.966 ± 0.000	14.01 ± 0.07
$\kappa_{electron\ reco,\ ID}$		0.985 ± 0.000	13.80 ± 0.07
$\kappa_{electron\ likelihood}$		0.891 ± 0.000	12.30 ± 0.06
Data Quality		0.971 ± 0.005	11.95 ± 0.09
ε^{total}			11.95 ± 0.09

TABLE 3: Summary of the $t\bar{t} \to e + jets$ event preselection efficiencies and the corresponding κ factors, if applicable, for exactly three jets. Only statistical uncertainties are included.

Selection or κ	Events left	Exclusive selection efficiency[%]	Cumulative selection efficiency[%]
	242352		
# good jets ≥4	115765	47.77 ± 0.10	47.77 ± 0.10
Leading jet > 40 GeV	113896	98.39 ± 0.04	47.00 ± 0.10
Loose electron	47037	41.30 ± 0.15	19.41 ± 0.08
Muon veto	47031	99.99 ± 0.01	19.41 ± 0.08
2nd electron veto	47023	99.98 ± 0.01	19.40 ± 0.08
Vertex selection	46309	98.48 ± 0.06	19.11 ± 0.08
$\not\!\!E_T$ > 20 GeV	40960	88.45 ± 0.15	16.90 ± 0.08
Triangle selection	38568	94.16 ± 0.12	15.91 ± 0.07
Tight electron	34580	89.66 ± 0.16	14.27 ± 0.07
Trigger probability		0.968 ± 0.000	13.81 ± 0.07
$\kappa_{electron\ reco,\ ID}$		0.985 ± 0.000	13.60 ± 0.07
$\kappa_{electron\ likelihood}$		0.891 ± 0.000	12.12 ± 0.06
Data Quality		0.971 ± 0.005	11.78 ± 0.09
ε^{total}			11.78 ± 0.09

TABLE 4: Summary of the $t\bar{t} \to e + jets$ event preselection efficiencies and the corresponding κ factors, if applicable, for four or more jets. Only statistical uncertainties are included.

Selection or κ	Events left	Exclusive selection efficiency[%]	Cumulative selection efficiency[%]
	240919		
# good jets =3	94389	39.18 ± 0.10	39.18 ± 0.10
Leading jet > 40 GeV	93404	98.96 ± 0.03	38.77 ± 0.10
Loose muon	42437	45.43 ± 0.16	17.61 ± 0.08
2nd muon veto	42432	99.99 ± 0.01	17.61 ± 0.08
Electron veto	42389	99.90 ± 0.02	17.59 ± 0.08
Vertex selection	41740	98.47 ± 0.06	17.33 ± 0.08
$\not\!\!E_T > 25$ GeV	35977	86.19 ± 0.17	14.93 ± 0.07
Triangle selection	33520	93.17 ± 0.13	13.91 ± 0.07
Tight muon	29356	87.58 ± 0.18	12.19 ± 0.07
Trigger probability		0.877 ± 0.001	10.69 ± 0.06
$\kappa_{\mu\ ID\times\ acc\times\ cosmic\ veto}$		0.956 ± 0.001	10.22 ± 0.06
$\kappa_{\mu\ track}$		0.855 ± 0.001	8.73 ± 0.05
$\kappa_{\mu+jets\ iso\ corr}$		1.102 ± 0.000	9.63 ± 0.06
$\kappa_{\mathrm{Rat11<0.08\ and\ Rattrk<0.06}}$		1.002 ± 0.000	9.64 ± 0.06
Data Quality		0.971 ± 0.005	9.37 ± 0.07
ε^{total}			9.37 ± 0.07

TABLE 5: Summary of the $t\bar{t} \to \mu + jets$ event preselection efficiencies and the corresponding κ factors, if applicable, for exactly three jets. Only statistical uncertainties are included.

Selection or κ	Events left	Exclusive selection efficiency[%]	Cumulative selection efficiency[%]
	240919		
# good jets ≥4	116398	48.31 ± 0.10	48.31 ± 0.10
Leading jet > 40 GeV	115412	99.15 ± 0.03	47.90 ± 0.10
Loose muon	47516	41.17 ± 0.14	19.72 ± 0.08
2nd muon veto	47515	100.00± 0.00	19.72 ± 0.08
Electron veto	47479	99.92 ± 0.01	19.71 ± 0.08
Vertex selection	46833	98.64 ± 0.05	19.44 ± 0.08
$\not\!\!E_T > 25$ GeV	39867	85.13 ± 0.16	16.55 ± 0.08
Triangle selection	37054	92.94 ± 0.13	15.38 ± 0.07
Tight muon	32069	86.55 ± 0.18	13.31 ± 0.07
Trigger probability		0.878 ± 0.001	11.69 ± 0.06
$\kappa_{\mu\ ID\times\ acc\times\ cosmic\ veto}$		0.958 ± 0.001	11.20 ± 0.06
$\kappa_{\mu\ track}$		0.854 ± 0.001	9.56 ± 0.05
$\kappa_{\mu+jets\ iso\ corr}$		1.003 ± 0.000	9.59 ± 0.05
$\kappa_{\mathrm{Rat11<0.08\ and\ Rattrk<0.06}}$		1.002 ± 0.000	9.61 ± 0.05
Data Quality		0.971 ± 0.005	9.33 ± 0.07
ε^{total}			9.33 ± 0.07

TABLE 6: Summary of the $t\bar{t} \to \mu + jets$ event preselection efficiencies and the corresponding κ factors, if applicable, for four or more jets. Only statistical uncertainties are included.

N_{Jets}	$e+jets$	$\mu+jets$
= 1 jet	83.6 ± 0.5(stat) ± 3.5(sys)	91.5 ± 0.6(stat) ± 0.9(sys)
= 2 jets	84.6 ± 0.3(stat) ± 1.5(sys)	88.7 ± 0.3(stat) ± 0.7(sys)
= 3 jets	84.8 ± 0.3(stat) ± 0.1(sys)	87.3 ± 0.3(stat) ± 0.5(sys)
≥ 4 jets	84.0 ± 0.4(stat) ± 1.8(sys)	84.5 ± 0.4(stat) ± 2.2(sys)

TABLE 7: ε_{sig} for different jet multiplicities in both channels, with their respective statistical and systematical errors (%).

V. BACKGROUNDS

In this section we describe the methods used to extract the $t\bar{t}$ signal and estimate background contributions which pass the preselection as discussed in Sect. IV. The backgrounds can be subdivided into two components:

- **Instrumental background:** Multijet background, strong production of four or more jets, with fake $\not\!\!E_T$ reconstruction and a fake tight electron by electromagnetic jets, punch-through fake muons, photons with a random track or real muons but fakely isolated from semi-leptonic b-decays with non-reconstructed b-jet.
- **Physics background:** Radiative W production accompanied by four or more jets (l+jets).

A. Instrumental Background: Multijet Background

The Matrix Method is used to estimate how many events in the preselected sample contain a fake lepton (originating from multijet production) and how many events have a real isolated lepton (like the ones originating from $t\bar{t}$ or W+jets events) in the data sample.

For the Matrix Method, two samples are defined for each jet multiplicity ($n = 1, 2, 3, \geq 4$) as follows: The **Tight Sample** is the sample after all preselection cuts are applied. It is a subset of the **Loose Sample** which is selected with the same preselection but requiring loose leptons instead of tight, thus omitting the tight electron likelihood or muon isolation requirements.

The number of events in the loose and tight samples are denoted as N_ℓ and N_t, respectively. $N^{\mathrm{W+t\bar{t}}}$ denotes the combined number of W+jets and $t\bar{t}$ events in the loose sample; N^{QCD} corresponds to the number of multijet events in the loose sample. ε_{sig} is the efficiency for a real lepton to pass the tight lepton selection; ε_{QCD} is the efficiency for a fake lepton to pass the tight lepton selection. With these definitions, one can write the following equations:

$$\begin{aligned} N_\ell &= N^{\mathrm{W+t\bar{t}}} + N^{\mathrm{QCD}} \\ N_t &= \varepsilon_{sig} N^{\mathrm{W+t\bar{t}}} + \varepsilon_{QCD} N^{\mathrm{QCD}} \end{aligned} \quad (1)$$

Solving this linear system for N^{QCD} and $N^{\mathrm{W+t\bar{t}}}$ yields:

$$N_t^{\mathrm{W+t\bar{t}}} = \varepsilon_{sig} \frac{N_t - \varepsilon_{QCD} N_\ell}{\varepsilon_{sig} - \varepsilon_{QCD}} \quad \text{and} \quad N_t^{\mathrm{QCD}} = \varepsilon_{QCD} \frac{\varepsilon_{sig} N_\ell - N_t}{\varepsilon_{sig} - \varepsilon_{QCD}}. \quad (2)$$

The efficiency ε_{sig} for true leptons in the signal jet multiplicity bin is obtained from the corresponding W+jets and $t\bar{t}$ MC samples. The values for ε_{sig} for different jet multiplicities are summarized in Table 7 [33].

The efficiency ε_{QCD} for fake leptons to pass the tight isolation selection, is measured directly from data in the low $\not\!\!E_T$ region ($\not\!\!E_T < 10$ GeV) [34]:

- e+jets : 19.5 ± 0.4 (stat) ± 1.7 (syst) %
- μ+jets : 27.2 ± 1.3 (stat) ± 5.2 (syst) %

The composition of the preselected sample as determined by the Matrix Method is given in Tables 8 and 9.

The systematic uncertainty on ε_{QCD} is derived from the observed dependence of the fake rate on the lepton p_T: The ε_{QCD} vs. lepton p_T distributions from the second inclusive jet multiplicity bin for all trigger list versions separately (e+jets) or combined (μ+jets) are folded with the corresponding QCD sample's p_T spectrum (loose not tight signal

selection). The result is then compared with the fake rate obtained without folding in the p_T distribution yielding the central value. For e+jets, the biggest deviation observed for a single trigger list is 1.7%.

In case of the μ+jets sample due to lack of statistics only the difference from p_T folding using all trigger lists together is used, yielding 5.2% (the sample statistics for multijets background is a factor of 8 lower in the μ+jets case, making differential studies more difficult).

B. Physics Background

Contributions of all physics backgrounds except for W+jets are estimated based on their NLO cross section as follows.

- Single top production in s and $t-$channels. To normalize the number of events of s- (t-) channel, we use the NLO cross section 0.88 (1.98) pb with 12.5% uncertainty [35].
- Diboson production: $WW \rightarrow l$+jets, $WZ \rightarrow l$+jets, $WZ \rightarrow jjl\bar{l}$, $ZZ \rightarrow jjl\bar{l}$. To normalize this sample, we use the NLO cross section 12.0 (WW), 3.68 (WZ), 1.42 (ZZ) pb with 20% uncertainty [36], individually.
- $Z + jets$: We apply the Z p_{T}reweighting described in [37]. We also multiply the Monte Carlo weights by a k factor of 1.23, and the Zbb and Zcc samples by and additional heavy flavor scale factor of 1.35. The NLO cross section uncertainty is 15% [38].

The relative normalization of W (or Z) + $b\bar{b}/c\bar{c}/q\bar{q}$ samples from the ALPGEN MC generator has to be corrected for NLO effects. We apply a heavy flavor scale factor of 1.17 ± 0.18 to the Wbb and Wcc samples, which was obtained by comparing MC and data for l+jets events with two jets [26]. To estimate the W+jets background contribution in the sample, we subtract the $t\bar{t}$, single top, diboson and Z+jets contributions from $N_t^{t\bar{t}+W}$ in each jet multiplicity bin using their NLO cross sections and normalize the W+jets MC samples ($Wb\bar{b}$ +$Wc\bar{c}$ +Wjj) to the remaining number of events.

Figures 1 and 2 show the distributions of the W transverse mass separately for each lepton flavor and jet multiplicity after the matrix method has been applied to normalize the W+jets and multijet backgrounds.

	N_l	N_t	N_t^{tt+W}	N_t^{QCD}	$\varepsilon_{\mathrm{sig}}$ (%)	$\varepsilon_{\mathrm{QCD}}$ (%)
$\mathrm{N_{jet}} = 1$	22398	15863	14992.4± 221.4	870.6±221.4	83.6	19.5
$\mathrm{N_{jet}} = 2$	10377	6043	5223.5±102.9	819.5±102.9	84.6	19.5
$\mathrm{N_{jet}} = 3$	2592	1300	1031.8±34.4	268.2±34.4	84.8	19.5
$\mathrm{N_{jet}} \geq 4$	618	320	259.8±10.1	60.2±10.1	84.0	19.5

TABLE 8: Number of preselected events in the loose and tight samples and the expected contribution from QCD and W-like events obtained with the Matrix Method in different jet multiplicity bins for the e+jets analysis.

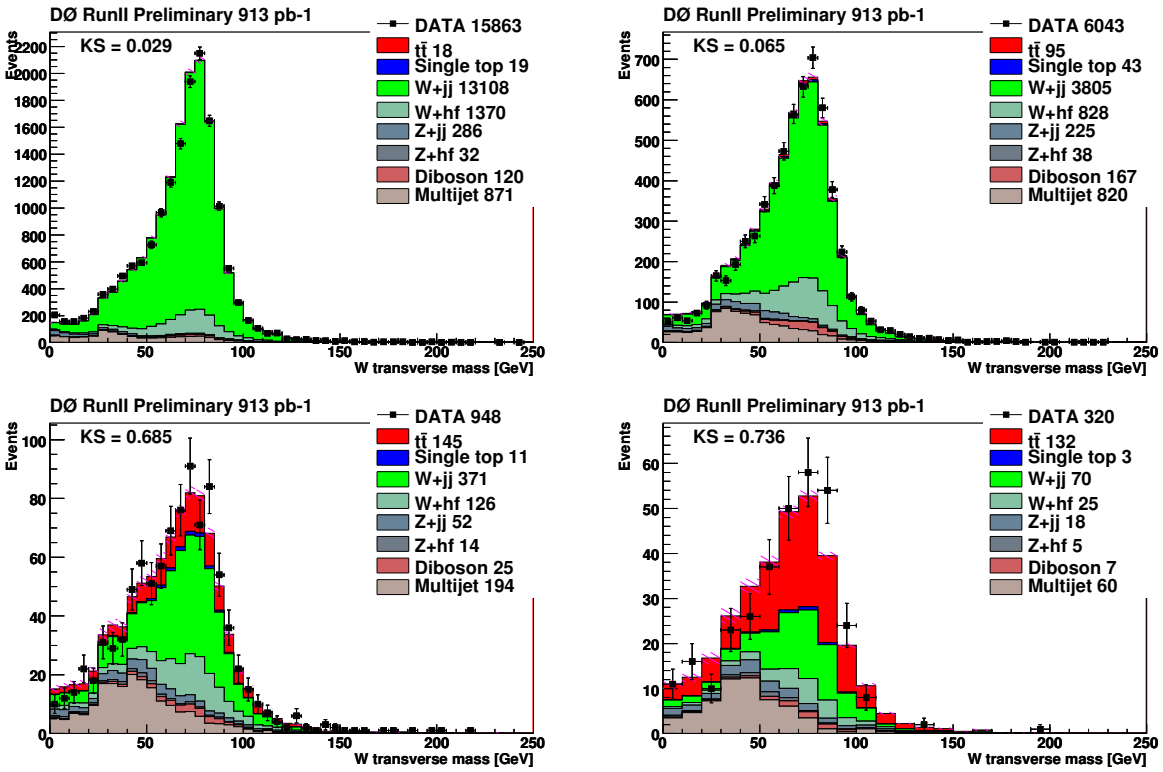

FIG. 1: $e\nu$ transverse mass distribution for the preselected sample with estimated fractions of $Wb\overline{b}$ $+Wc\overline{c}$ $+Wjj$, single top, $t\overline{t}$ and multijet events obtained from the Matrix Method. The plots show the data for different jet multiplicities: =1 jet (top left), =2 jets (top right), = 3 jets (bottom left), and $\geq$ 4 jets (bottom right).

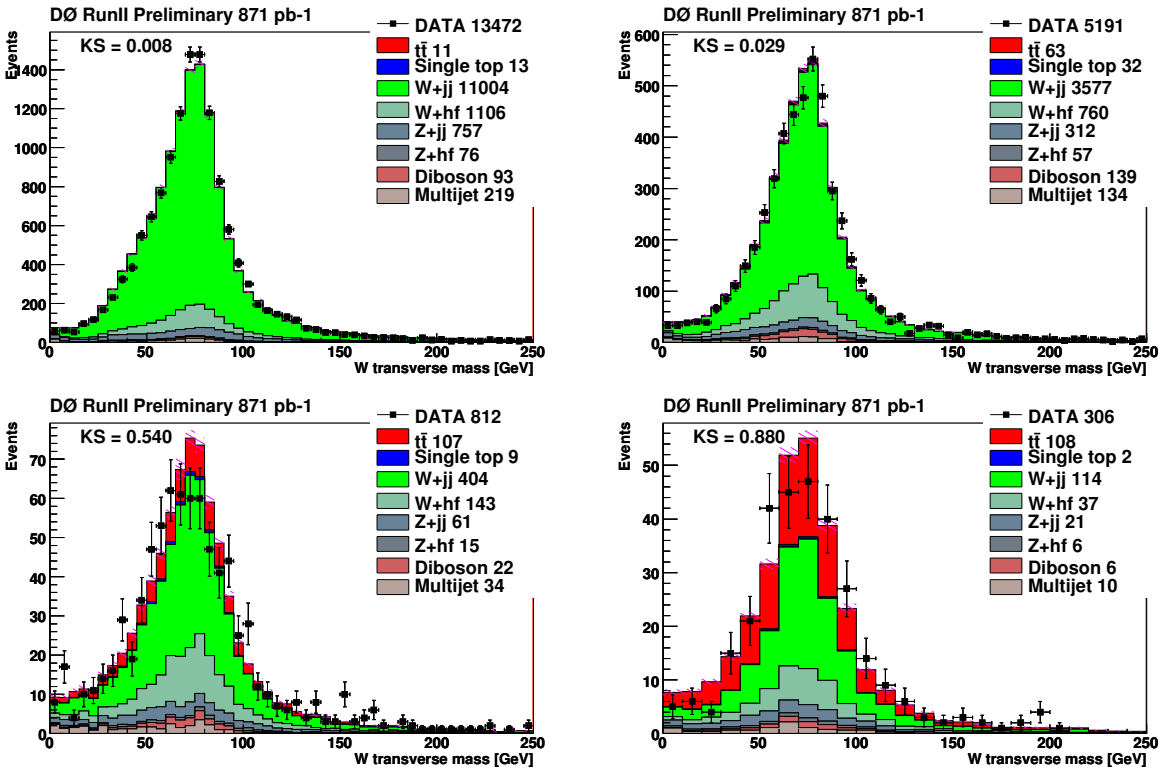

FIG. 2: $\mu\nu$ transverse mass distribution for the preselected sample with estimated fractions of $Wb\overline{b}$ +$Wc\overline{c}$ +Wjj , single top, $t\overline{t}$ and multijet events obtained from the Matrix Method. The plots show the data for different jet multiplicities: =1 jet (top left), =2 jets (top right), = 3 jets (bottom left), and $\geq$ 4 jets (bottom right).

	N_l	N_t	N_t^{tt+W}	N_t^{QCD}	$\varepsilon_{\rm sig}$ (%)	$\varepsilon_{\rm QCD}$ (%)
$N_{\rm jet} = 1$	15289	13472	13253.1±90.9	218.9±90.9	91.5	27.2
$N_{\rm jet} = 2$	6194	5191	5057.0 ±44.0	134.0±44.0	88.7	27.2
$N_{\rm jet} = 3$	1389	1120	1078.1 ±13.9	41.9 ±13.9	87.3	27.2
$N_{\rm jet} \geq 4$	388	306	295.6 ±5.7	10.4 ±5.7	84.5	27.2

TABLE 9: Number of preselected events in the loose and tight samples and the expected contribution from QCD and W-like events obtained with the Matrix Method in different jet multiplicity bins for the μ+jets analysis.

VI. TOPOLOGICAL ANALYSIS

The purpose of the preselection is to extract the $W \rightarrow l$+jets events with maximum efficiency while rejecting the multijet background.

None of the topological variables has enough discrimination power by itself to place a straight selection on either of them in order to separate the $t\bar{t}$ signal from the background. Therefore the event information contained in the topological variables is combined in a likelihood discriminant.

We have chosen to use a 2-class likelihood with $t\bar{t}$ as signal and physics backgrounds (MC) as background instead of a 3-class likelihood where in addition to the physics background class multiejts background class would be considered since the available multijet background sample is very limited in statistics and the fraction of multijets in the preselected sample is small enough($< 10\%$) which is smaller than statistical uncertainy in likelihood discriminant.

The signal sample consists of $t\bar{t} \rightarrow l$+jets and small contribution from $t\bar{t} \rightarrow ll$+jets where the second lepton was not reconstructed or didn't pass the preselection requirements. Total efficiency is the sum of these two processes. The physics background consists of single top, W+jets, W$b\bar{b}$, W$c\bar{c}$, Z+jets, Z$b\bar{b}$, Z$c\bar{c}$ and diboson as described in V B.

A. Topological Likelihood Discriminant

The 3 jet samples are dominated by W+jets backgrounds. We therefore apply a cut on $\sum$ Jet $p_T > 120$ GeV in these events to reduce backgrounds. In order to avoid overtraining of the likelihood only a fraction of the events is used to build the likelihood. It was found that a half of the $t\bar{t}$ signal and W+jets background samples is sufficient. However, the full sample is used to evaluate the likelihood discriminant in order to minimize the statistical uncertainty and to guarantee that the same events are used both for the central value and for the systematically varied samples. We used **TMVA** [39] root class (v3.8.7) to build likelihood discriminant. The likelihood output $\mathcal{L}_i$ for each event i is given by

$$\mathcal{L}_i \;=\; \frac{L_S(i)}{L_S(i) + L_B(i)} \tag{3}$$

Here the signal and background likelihoods, L_S, L_B, are products of the corresponding probability densities, p_S, p_B of the $N_{variable}$ discriminating variables used:

$$L_S(i) \;=\; \prod_{j=1}^{N_{variable}} p_{Sj}(i) \tag{4}$$

and accordingly for L_B. TMVA uses polynomial splines to estimate the probability density functions (PDF) obtained from the distributions of the training variables.

The most objective way to determine the power of a variable, and establish a ranking, is to retrain a classifier with subset of variables, and remove those that bring the least improvement in classification power. This is realised for Likelihood, where Δ separation determines the loss of separation with a given variable removed from the overall likelihood [39]. The Tables 10- 13 show the rank of variables based on Δ separation. For samples with jet multiplicity n we also quote the result of a Kolmogrov-Smirnov test for the control plots in the sample with a jet multiplicity $n-1$ to indicate how well the distribution is modelled by the simulation.

Rank	Variable	Δ Separation	Kolmogrov Test result for 2 jet sample
1	metHTplusLepton	1.124e-01	0.641
2	HT	1.094e-01	0.521
3	HT2p	9.585e-02	0.036
4	HTplusLepton	9.346e-02	0.851
5	Et3	8.485e-02	0.983(*)
6	Jet1 η	4.775e-02	0.474
7	Jet1Jet2DeltaR	4.616e-02	0.018
8	Sphericity	4.344e-02	0.183
9	maxJetEta	3.918e-02	0.002
10	Aplanarity	3.563e-02	0.171
11	Jet2 η	3.023e-02	0.287
12	minDijetDeltaR	2.324e-02	0.005
13	H	2.103e-02	0.039
14	Hz	1.757e-02	0.009
15	DphiLMET	1.679e-02	0.141
16	LeptonJetDeltaR	8.494e-03	0.372
17	DphiJMET	6.000e-03	0.270

TABLE 10: Rank of variables for e+jets sample with 3 jets. Jet1 is the leading jet in p_T and Jet2 is second leading jet. For Et3 we quote the KS from the control plot with 3 jet event because the variable is not define for 2 jets.

Rank	Variable	Δ Separation	Kolmogrov Test result for 3 jet sample
1	Et3	1.200e-01	0.983
2	HT2p	1.180e-01	0.423
3	HT	1.177e-01	0.896
4	metHTplusLepton	1.176e-01	0.893
5	HTplusLepton	1.045e-01	0.988
6	Aplanarity	6.111e-02	0.200
7	Sphericity	6.032e-02	0.912
8	maxJetEta	5.213e-02	0.117
9	Jet1 η	4.406e-02	0.998
10	H	4.149e-02	0.349
11	Jet1Jet2DeltaR	4.127e-02	0.786
12	Jet2 *eta*	3.775e-02	0.620
13	Hz	3.137e-02	0.315
14	minDijetDeltaR	2.534e-02	0.254
15	DphiLMET	2.317e-02	0.274
16	LeptonJetDeltaR	1.592e-02	0.385
17	DphiJMET	8.244e-03	0.926

TABLE 11: Rank of variables for the e+jets sample with 4 or more jets.

Rank	Variable	Δ Separation	Kolmogrov Test result for 2 jet sample
1	HT	1.159e-01	0.062
2	HT2p	1.040e-01	0.002
3	metHTplusLepton	1.021e-01	0.750
4	Et3	1.016e-01	0.829(*)
5	HTplusLepton	8.818e-02	0.495
6	Sphericity	5.315e-02	0.021
7	Aplanarity	5.149e-02	0.020
8	Jet1Jet2DeltaR	5.104e-02	0.000
9	Jet1 η	3.927e-02	0.305
10	maxJetEta	3.633e-02	0.000
11	Jet2 η	3.406e-02	0.084
12	minDijetDeltaR	2.728e-02	0.000
13	Hz	2.136e-02	0.000
14	H	2.117e-02	0.024
15	DphiLMET	1.986e-02	0.051
16	LeptonJetDeltaR	9.230e-03	0.044
17	DphiJMET	5.788e-03	0.992

TABLE 12: Rank of variables for the μ+jets sample with 3 jets. For Et3 we quote the KS from the control plot with 3 jet event because the variable is not define for 2 jets.

Rank	Variable	Δ Separation	Kolmogrov Test result for 3 jet sample
1	HT	1.195e-01	0.814
2	HT2p	1.188e-01	0.114
3	Et3	1.132e-01	0.829
4	metHTplusLepton	1.041e-01	0.979
5	HTplusLepton	9.346e-02	0.850
6	Sphericity	7.628e-02	0.763
7	Aplanarity	7.333e-02	0.997
8	Jet1Jet2DeltaR	5.296e-02	0.803
9	maxJetEta	5.122e-02	0.056
10	H	4.121e-02	0.369
11	Jet1 η	3.968e-02	0.501
12	Jet2 η	3.472e-02	0.836
13	Hz	3.396e-02	0.277
14	DphiLMET	3.320e-02	0.993
15	minDijetDeltaR	2.289e-02	0.493
16	LeptonJetDeltaR	1.352e-02	0.868
17	DphiJMET	1.083e-02	0.885

TABLE 13: Rank of variables for the μ+jets sample with 4 or more jets.

Since the variation of systematic uncertainty on the different set of variables is smaller than the statistical uncertainty, we choose the variables based on the rank tables.

The criteria for the choice of the topological variables are the following:

- Use variables with a large separation power between signal and background.
- In case the Δ separation is similar between single variable and the combination of variables, instead of requiring each single variable to be insensitive against systematic uncertainties, the set of variables is chosen such that the combination of the variables is robust against the systematic variations.
- If possible, use variables which are not correlated or which have a small correlation. Correlated variables add only new information when the correlation is different for signal and background. However, variables are subject to statistical fluctuations and they enlarge the statistical uncertainties even if they add no new information.
- Reasonable Kolmogrov test result for $(n-1)$ jet sample.

B. Topological Variables for Likelihood Discriminants

Based on Rank and Kolmogrov test in Tables 10- 13, we choose following variables for likelihood discriminant.

Channel	Variables for Likelihood Discriminant
e+jets = 3	Et3, HT2p, Sphericity, Aplanarity, LeptonJetDeltaR, DphiJMET
e+jets $\geq$ 4	Et3, HT2p, Aplanarity, Sphericity, Jet1Jet2DeltaR, LeptonJetDeltaR
μ+jets = 3	Et3, metHTplusLepton, DphiLMET, LeptonJetDeltaR, DphiJMET
μ+jets $\geq$ 4	Et3, Sphericity, Aplanarity, Jet1Jet2DeltaR, LeptonJetDeltaR, DphiLMET

TABLE 14: Variables for likelihood Discriminant for each channel

where the definition of combination of variables are

metHTplusLepton: Scalar sum of the p_T of the jets, lepton p_T and $\not\!\!E_T$.

HT The scalar sum of the p_T of the jets.

Hz Z component of the scalar sum of the jets energy.

Et3: $\sum_{j=3}$Jet p_T

HT2p HT/Hz

Aplanarity: The normalized momentum tensor $\mathcal{M}$ is defined as:

$$\mathcal{M}_{ij} = \frac{\Sigma_o p_i^o p_j^o}{\Sigma_o |\vec{p^o}|^2}, \tag{5}$$

where $\vec{p^o}$ is the momentum-vector of a reconstructed object o, i and j are Cartesian coordinates. By standard diagonalization of $\mathcal{M}_{ij}$ one may find three eigenvalues $\lambda_1 \geq \lambda_2 \geq \lambda_3$, with $\lambda_1 + \lambda_2 + \lambda_3 = 1$. The aplanarity $\mathcal{A}$, a measure of the flatness of the event, is defined as $\mathcal{A} = \frac{3}{2}\lambda_3$, where λ_3 is the smallest eigenvalue of the normalized momentum tensor $\mathcal{M}$ (see Eq. 5). Therefore, it is defined in the range $0 \leq \mathcal{A} \leq 0.5$. The objects included in the sum are the jets and the lepton from the W decay. Large values of $\mathcal{A}$ are indicative of spherical events, whereas small values correspond to more planar events. $t\bar{t}$ events are quite spherical as is typical for the decay of a heavy object. W+jets and QCD events are more planar, primarily due to the fact that the jets in these events arise mainly from initial state radiation.

Sphericity: The sphericity $\mathcal{S}$ of the event is defined as

$$\mathcal{S} = \frac{3}{2}(\lambda_2 + \lambda_3), \tag{6}$$

where λ_2 and λ_3 are the smallest eigenvalues of the normalized momentum tensor $\mathcal{M}$ (see Eq. 5), so that $0 \leq \mathcal{S} \leq 1$. Sphericity is essentially a measure of the summed $p_\perp^2$ with respect to the event axis; a 2-jet event corresponds to $\mathcal{S} \approx 0$ and an isotropic event to $\mathcal{S} \approx 1$. $t\bar{t}$ events are quite isotropic as is typical for the decay of a heavy object. W+jets and QCD events are less isotropic, primarily due to the fact that the jets in these events arise from initial state radiation.

DphiLMET: The azimuthal opening angle between the lepton and the missing transverse energy.

DphiJMET: The azimuthal opening angle between the leading Jet and the missing transverse energy.

LeptonJetDeltaR: The ΔR between the direction of the leading Jet and the lepton.

Jet1Jet2DeltaR: The ΔR between the direction between two leading Jets.

Tables 3, 7, 11, 15 show the input variables Tables 4, 8, 12, 16 show the comparison between data and MC expectation with Kolmogrov test and Tables 5, 9, 13, 17 show the likelihood discriminant. Tables 6, 10, 14, 18 show templates for maximum likelihood fitting to estimate cross section in the data.

The normalized distributions of the the topological variables and relative referece distributions are shown in Figs. 3-6 for e+jets =3.

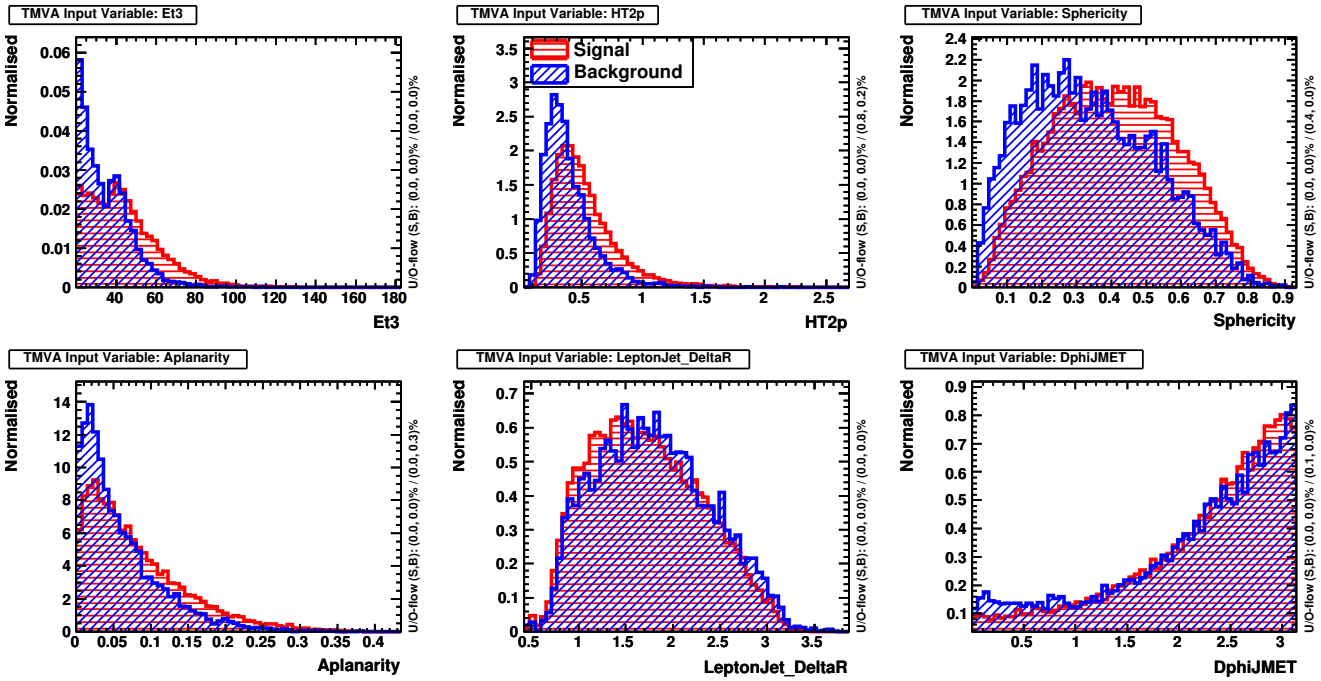

FIG. 3: Likelihood input distributions for $t\bar{t}$ and W+jets for the e+jets =3.

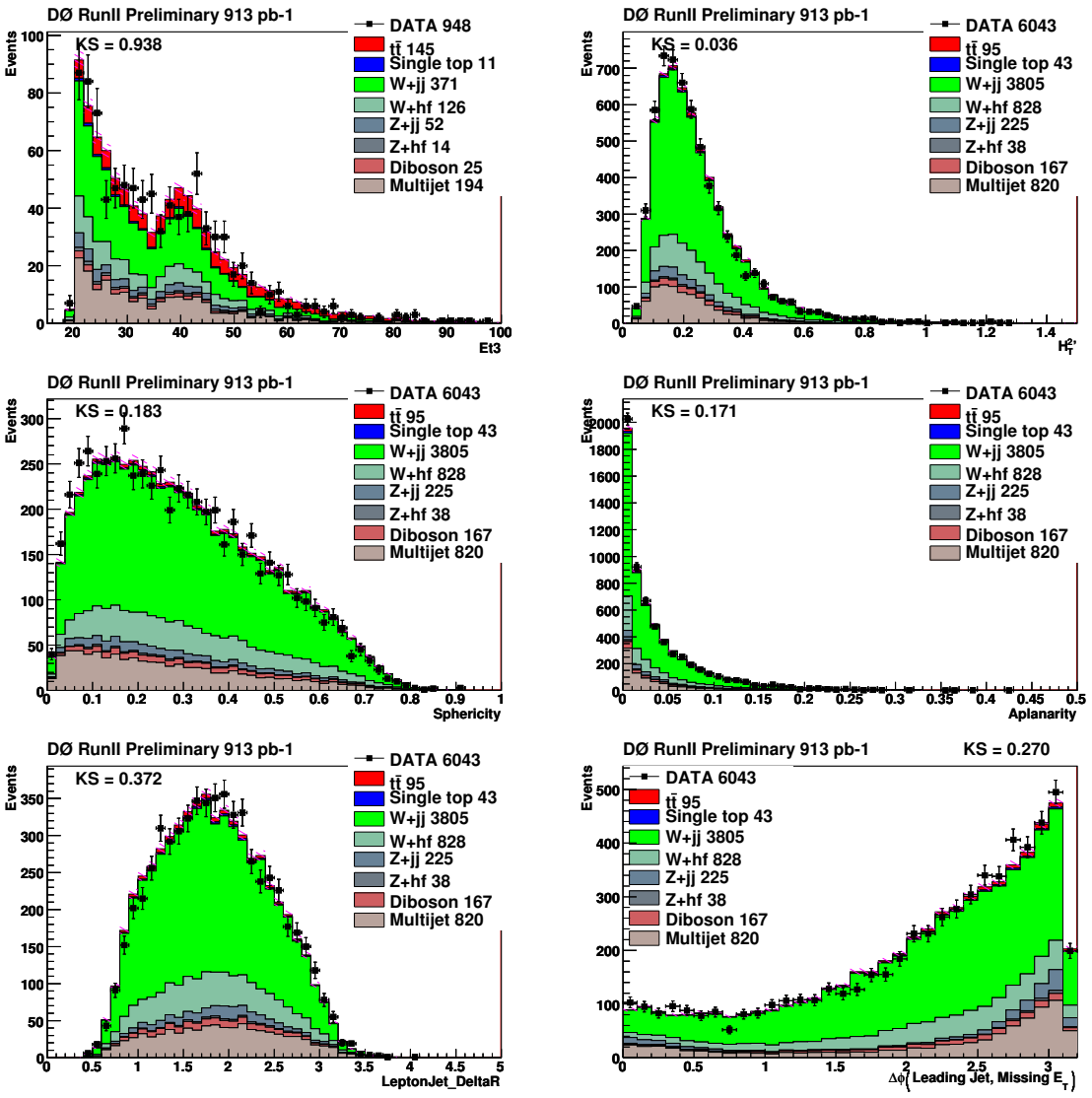

FIG. 4: Topological variables of Data compared with backgrounds estimation for $t\bar{t}$ and W+jets for the e+jets =2. (Et3 is from e+jets =3.)

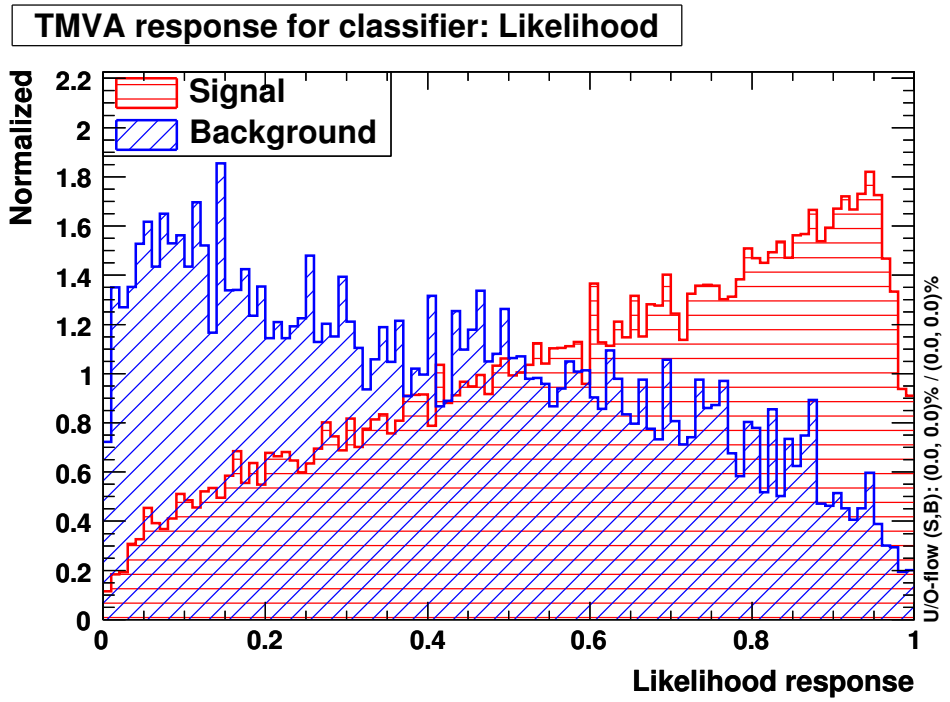

FIG. 5: Likelihood distributions for checking overtraining for $t\bar{t}$ and W+jets for the e+jets =3.

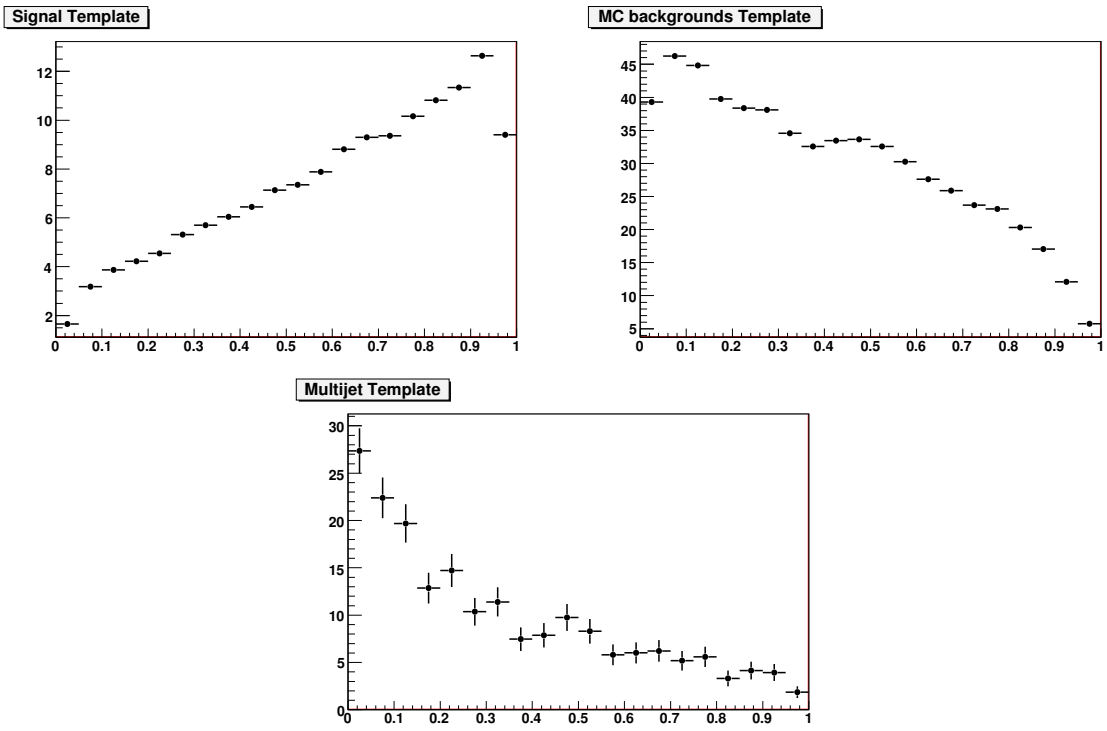

FIG. 6: Likelihood Template distribution used for Maximum Likelihood fitting for $t\bar{t}$ and W+jets for the e+jets =3.

The normalized distributions of the the six topological variables and relative referece distributions are shown in Figs. 7- 10 for e+jets $\geq$4.

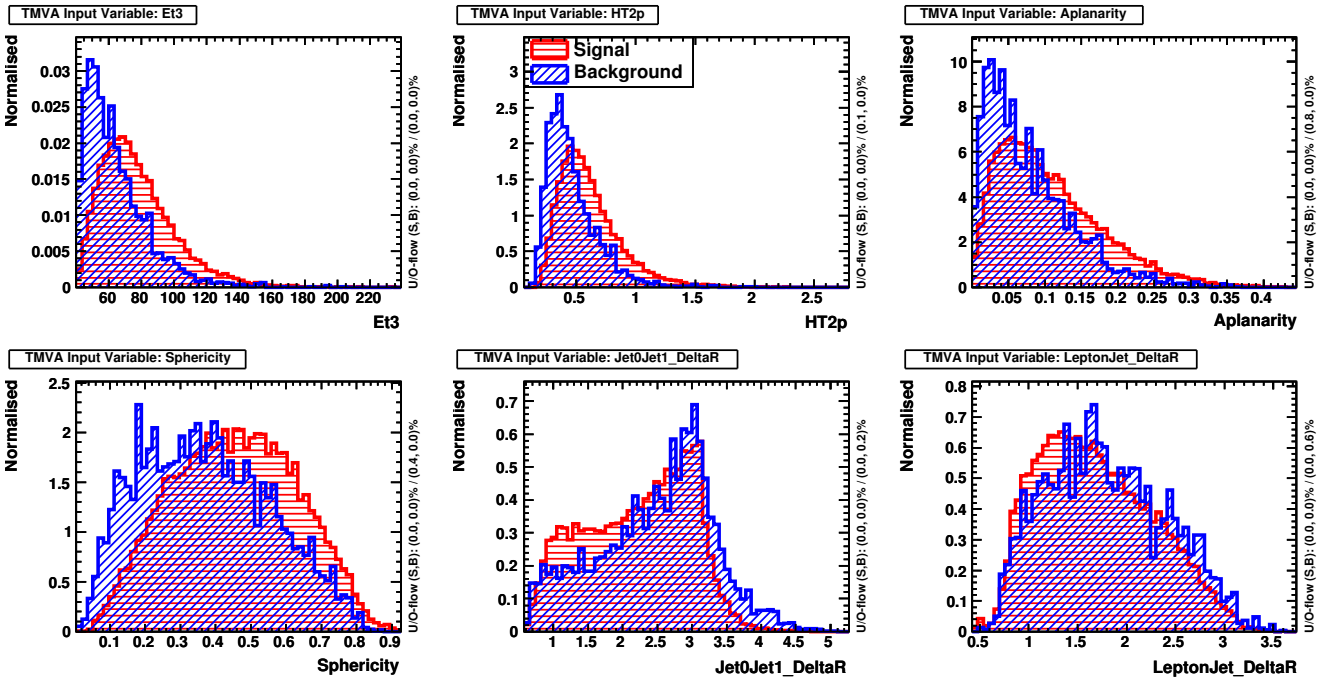

FIG. 7: Likelihood input distributions for $t\bar{t}$ and W+jets for the e+jets $\geq$4.

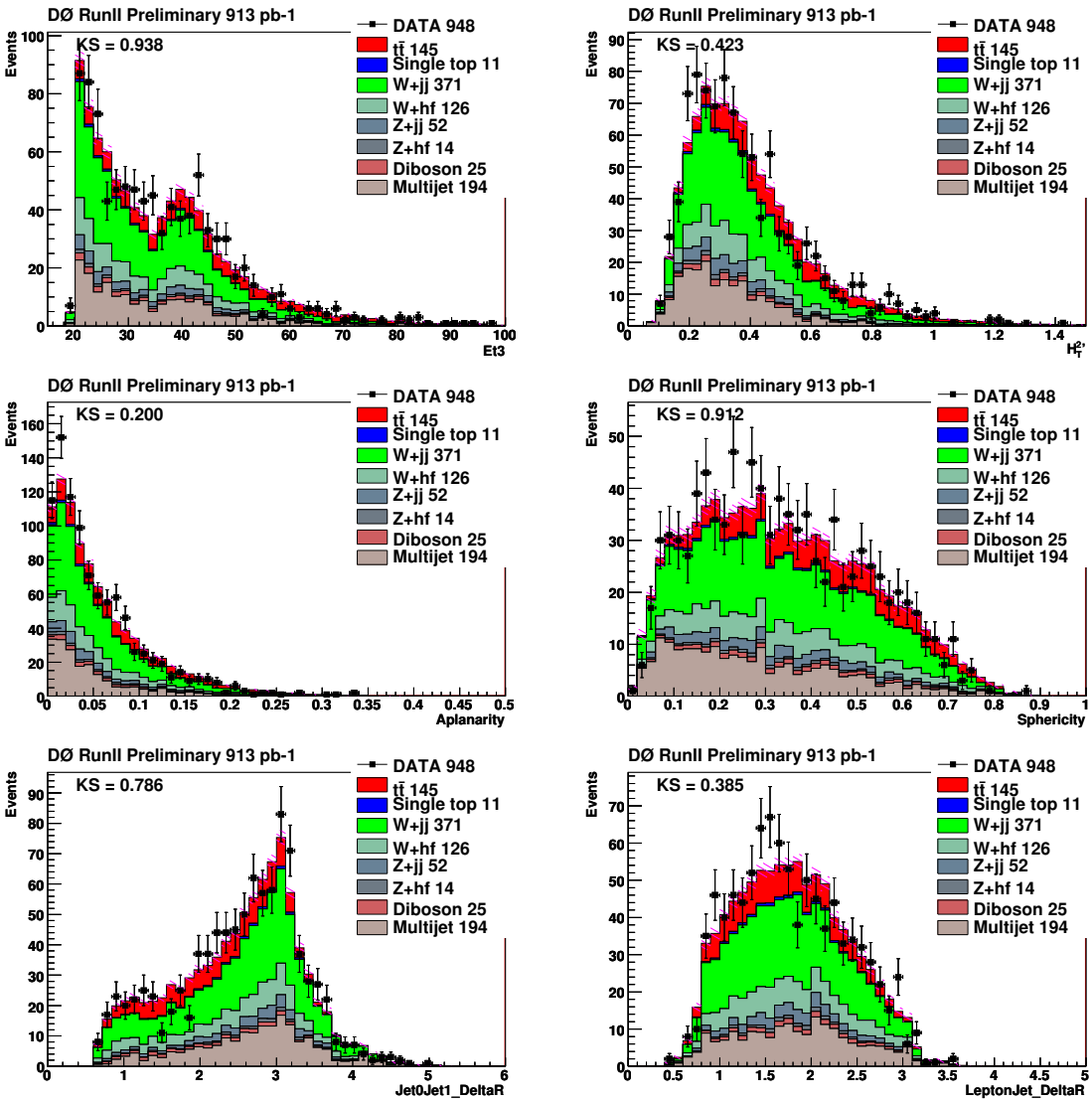

FIG. 8: Topological variables of Data compared with backgrounds estimation for $t\bar{t}$ and W+jets for the e+jets =3.

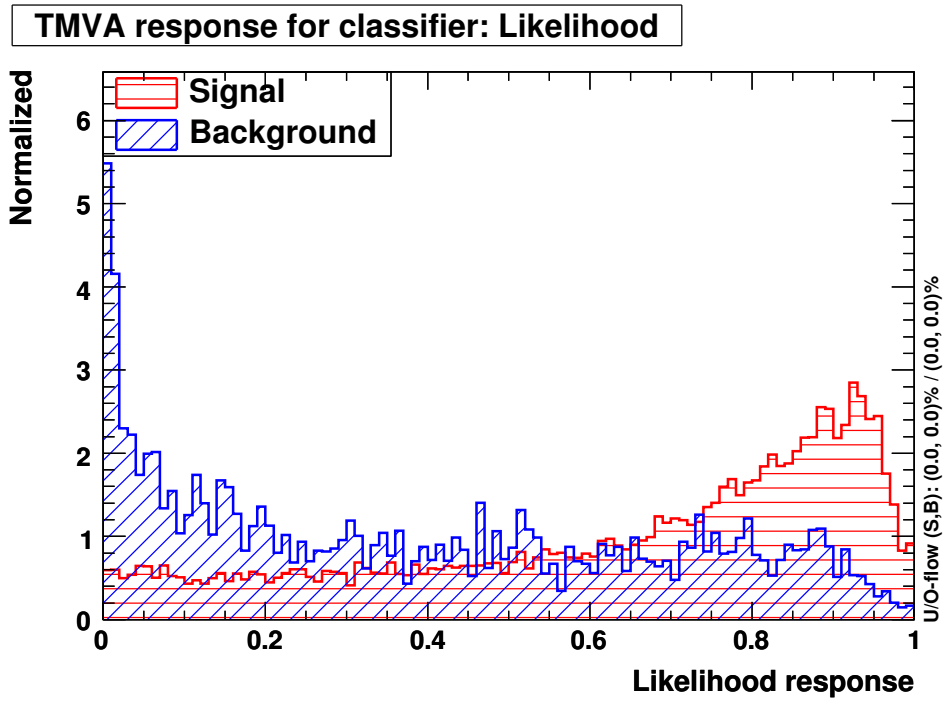

FIG. 9: Likelihood distributions for checking overtraining for $t\bar{t}$ and W+jets for the e+jets $\geq$4.

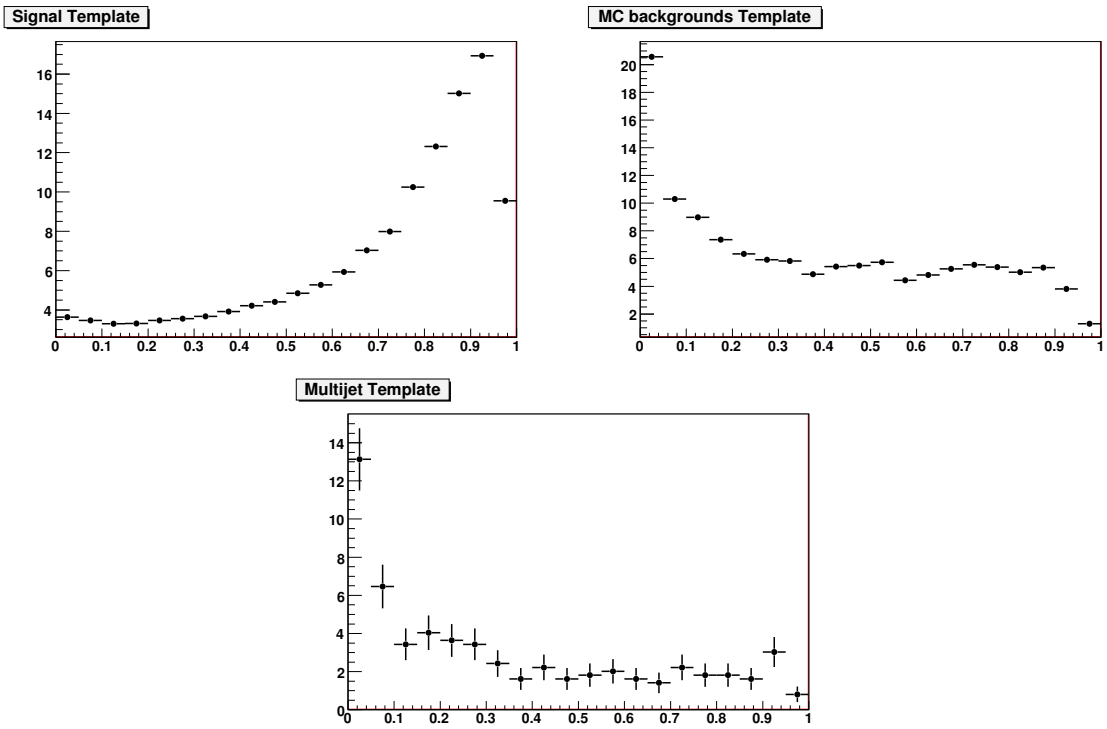

FIG. 10: Likelihood Template distribution used for Maximum Likelihood fitting for $t\bar{t}$ and W+jets for the e+jets $\geq$4.

The normalized distributions of the the six topological variables and relative referece distributions are shown in Figs. 11- 14 for μ+jets =3.

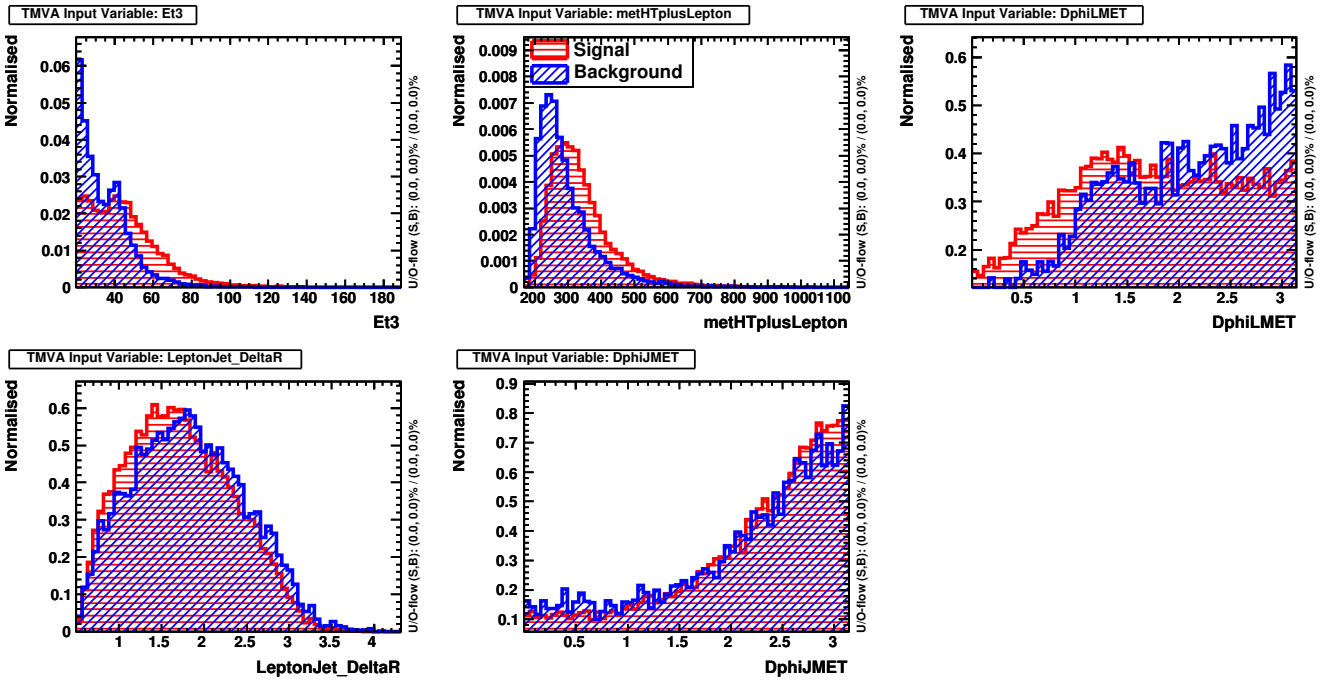

FIG. 11: Likelihood input distributions for $t\bar{t}$ and W+jets for the μ+jets =3.

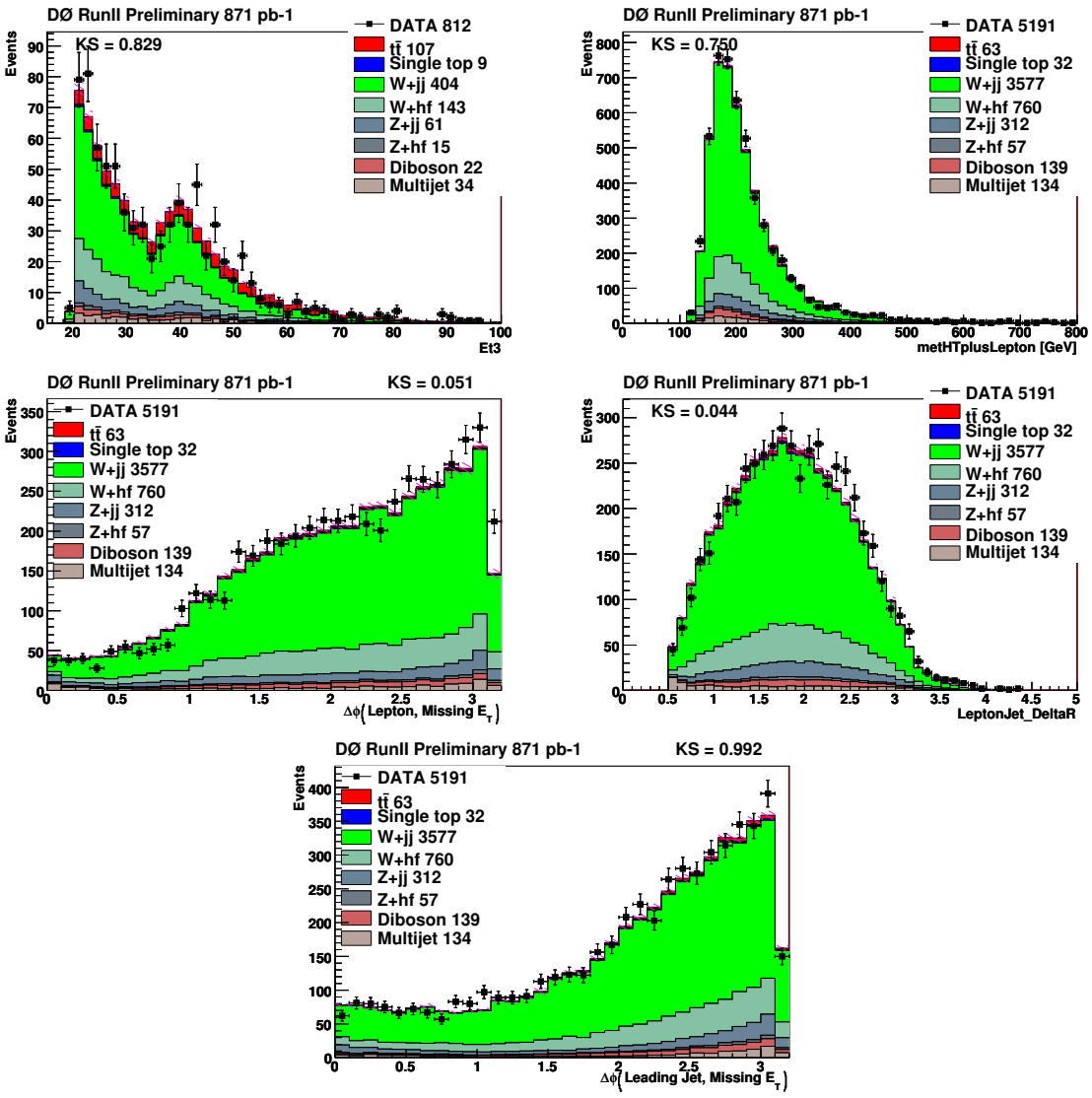

FIG. 12: Topological variables of Data compared with backgrounds estimation for $t\bar{t}$ and W+jets for the μ+jets =2. (Et3 is from μ+jets =3.)

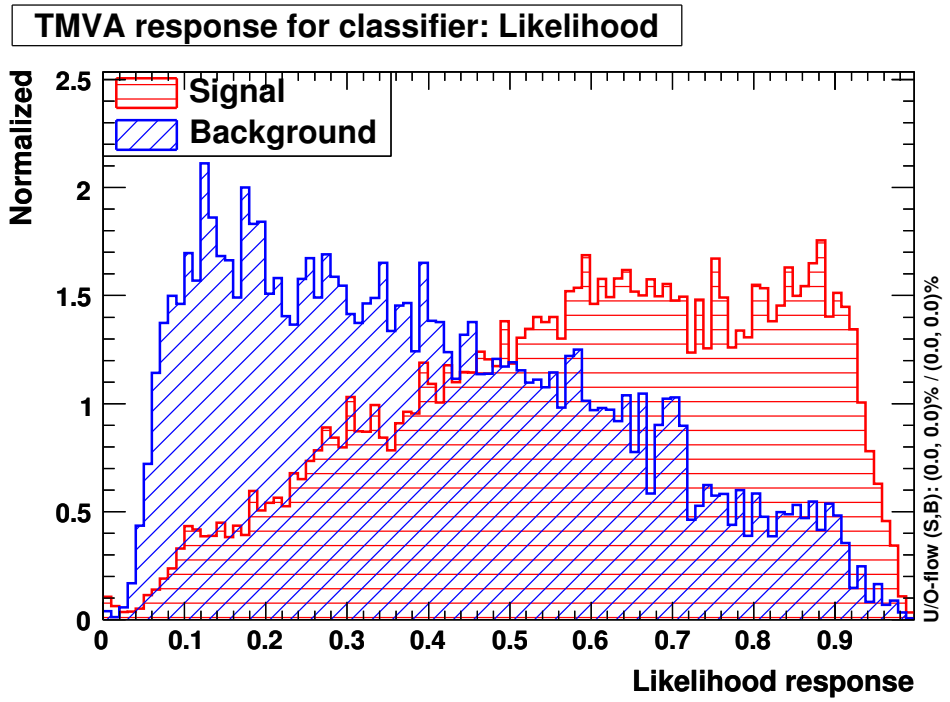

FIG. 13: Likelihood distributions for checking overtraining for $t\bar{t}$ and W+jets for the μ+jets =3.

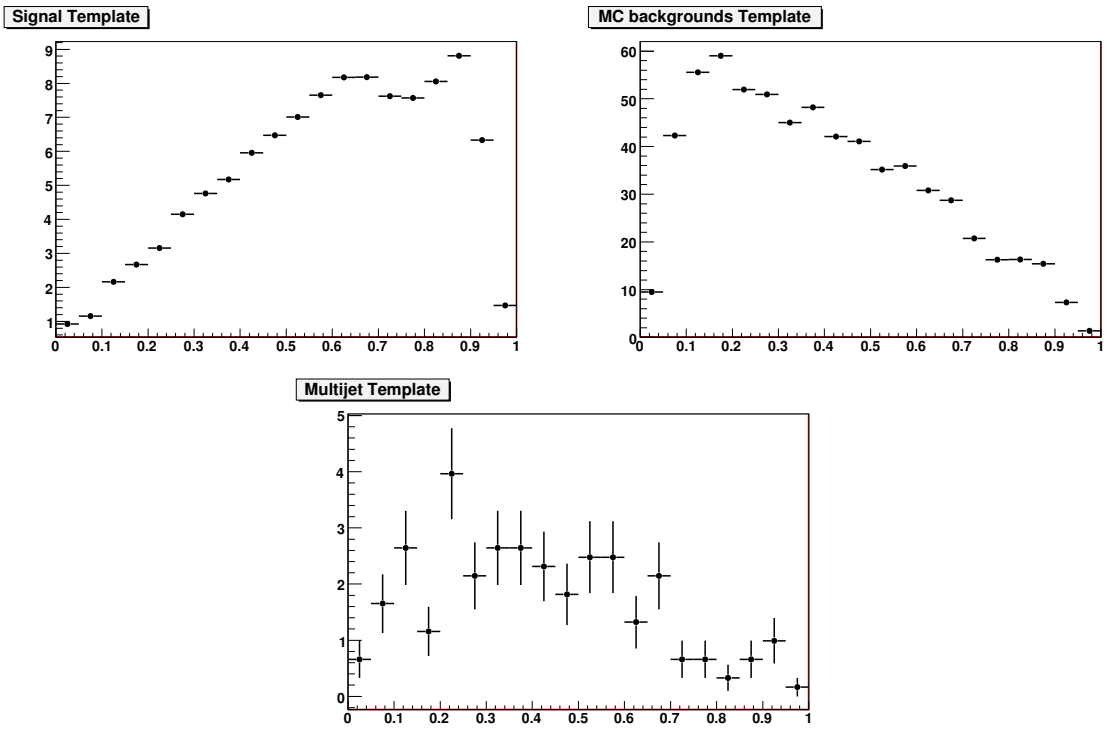

FIG. 14: Likelihood Template distribution used for Maximum Likelihood fitting for $t\bar{t}$ and W+jets for the μ+jets =3.

The normalized distributions of the the six topological variables and relative referece distributions are shown in Figs. 15- 18 for μ+jets $\geq$4.

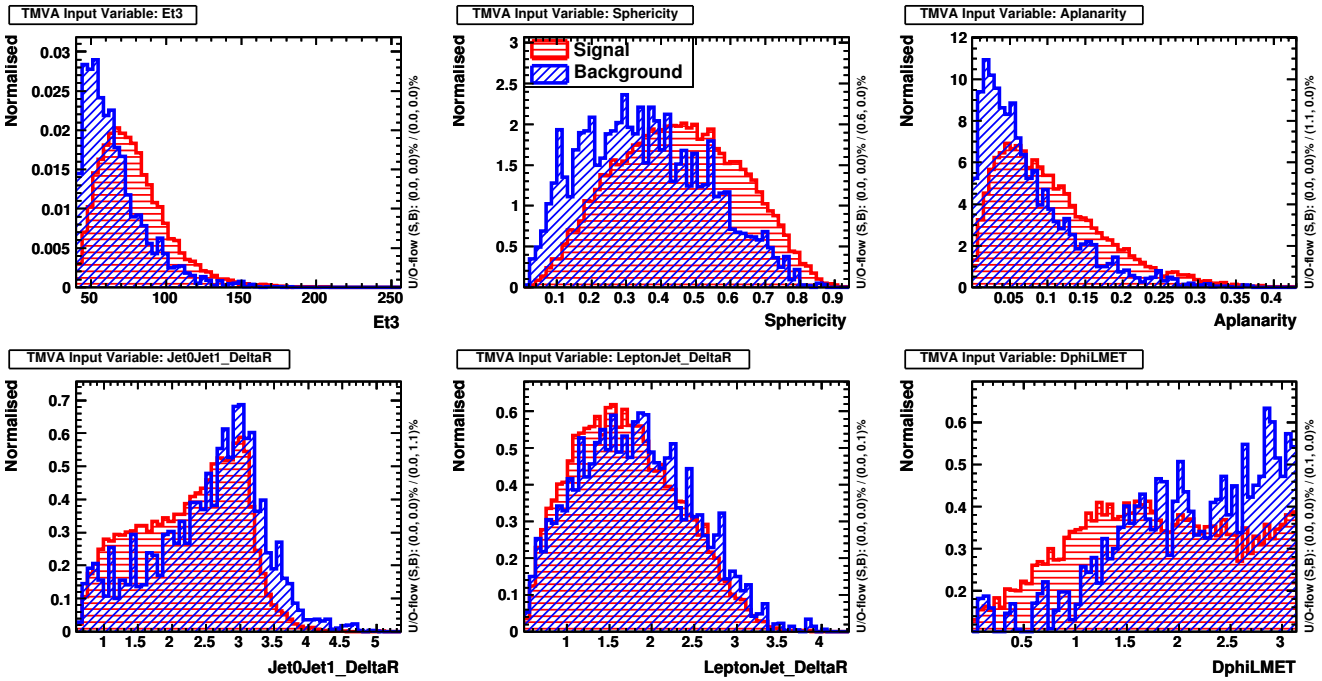

FIG. 15: Likelihood input distributions for $t\bar{t}$ and W+jets for the μ+jets $\geq$4.

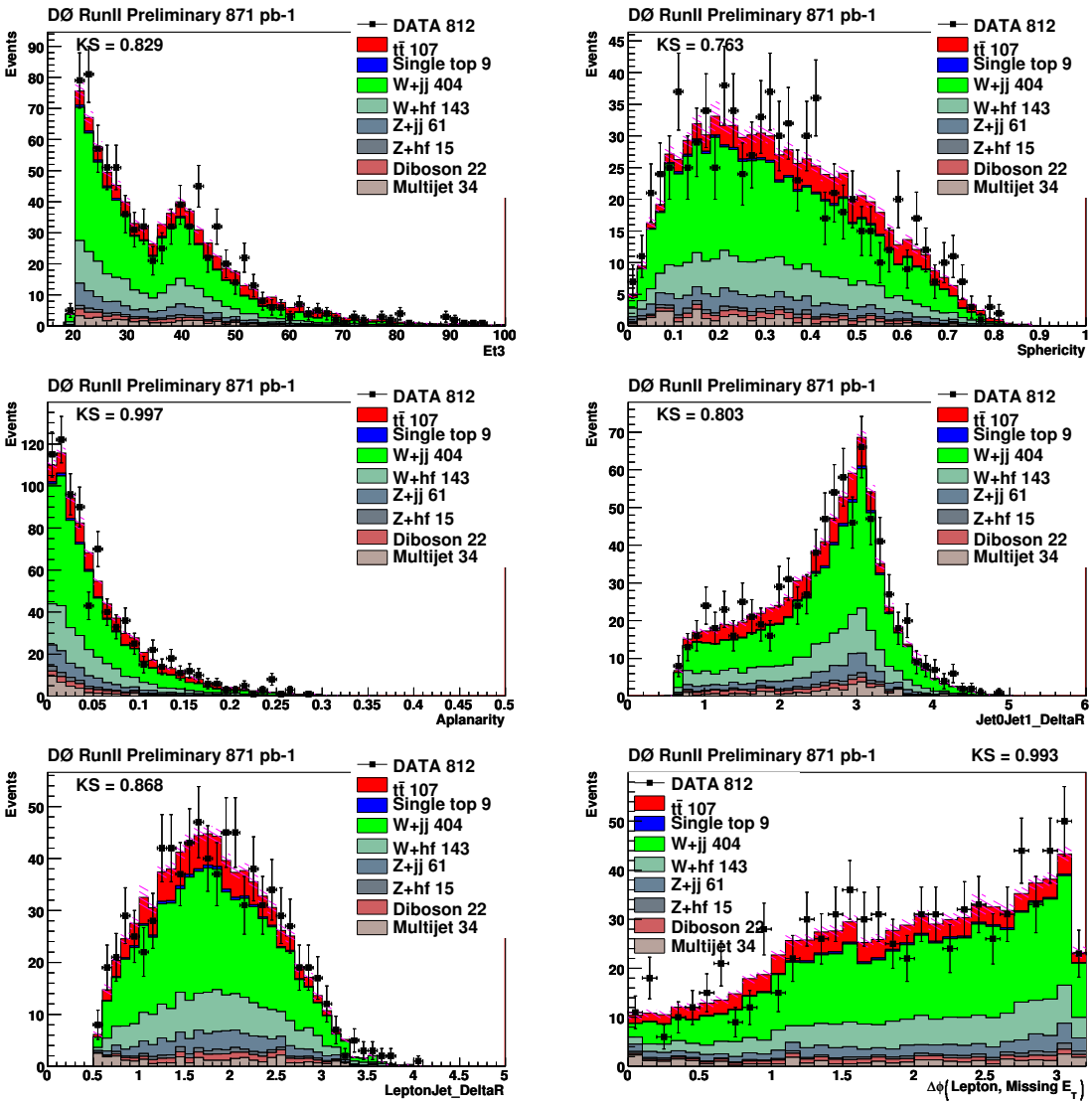

FIG. 16: Topological variables of Data compared with backgrounds estimation for $t\bar{t}$ and W+jets for the μ+jets =3.

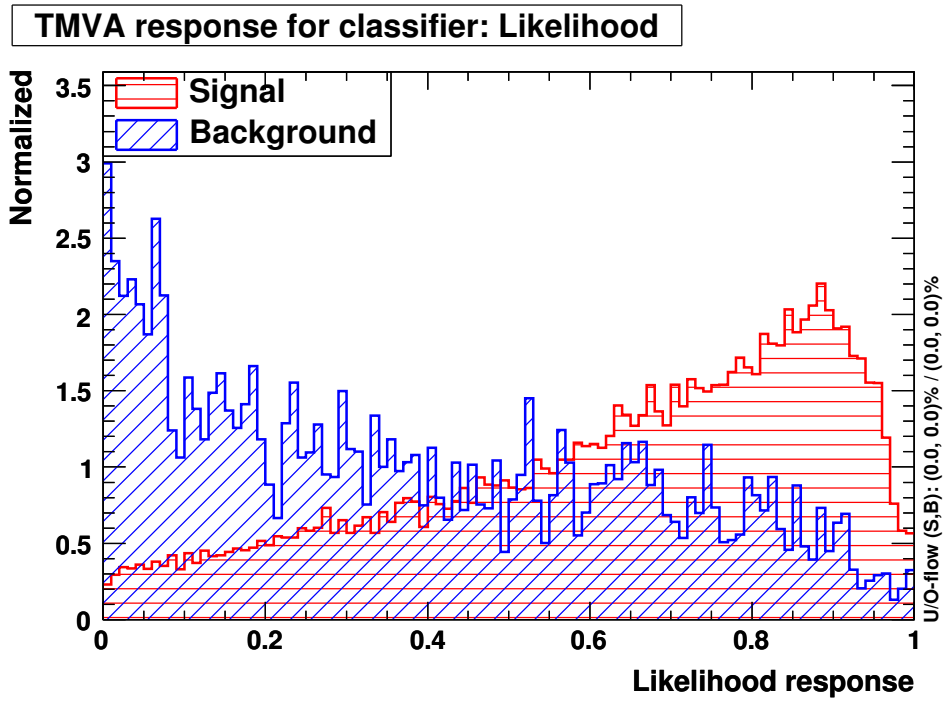

FIG. 17: Likelihood distributions for checking overtraining for $t\bar{t}$ and W+jets for the μ+jets $\geq$4.

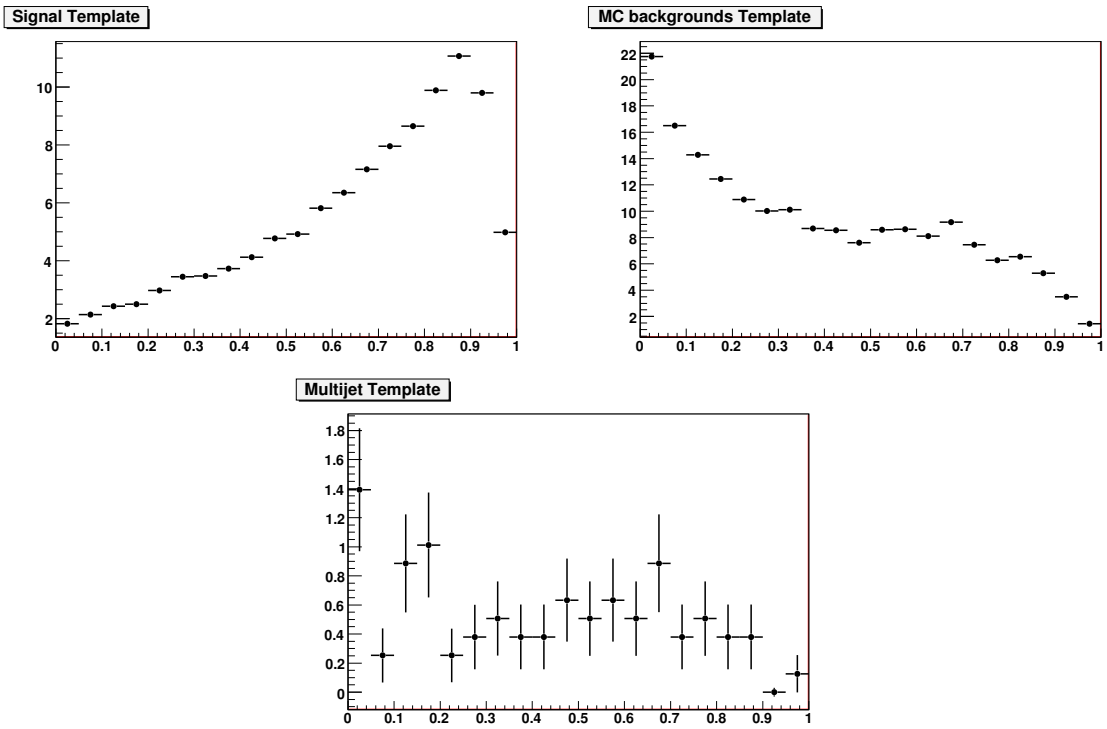

FIG. 18: Likelihood Template distribution used for Maximum Likelihood fitting for $t\bar{t}$ and W+jets for the μ+jets $\geq$4.

VII. CROSS-SECTION EXTRACTION PROCEDURE

The number of $t\bar{t}$ events in the preselected data sample can be directly extracted by performing a likelihood fit to the likelihood discriminant (see Sect. VI A) distribution in data using templates for the $t\bar{t}$ signal, the physics backgrounds, and the multijet background. However, the relative fractions of physics backgrounds and multijet background are already measured as a function of the $t\bar{t}$ cross-section by applying the matrix method that was discussed in Sect. V A. This circumstance allows to perform a fit where the number of $t\bar{t}$ ($N_t^{t\bar{t}}$), physics backgrounds (N_t^B) and multijet (N_t^{QCD}) in the tight (t) sample are allowed to float, but the relative fractions of MC backgrounds and Multijet are constrained by the matrix method measurement. The Topological likelihood defines in the following way for each channel:

$$L(N_t^{t\bar{t}}, N_t^B, N_t^{QCD}) = \left[\prod_i P(n_i^{obs}, \mu_i)\right] \cdot P(N_{\ell-t}^{obs}, N_{\ell-t}) \tag{7}$$

where $P(n, \mu)$ generically denotes the Poisson probability density function for n observed events given an expectation value of μ. In the first term of Eq. 7, i runs over all bins of the likelihood discriminant histogram, n_i^{obs} is the content of bin i as obtained in the preselected data sample, and μ_i is the expectation, which is a function of $N_t^{t\bar{t}}$, N_t^B and N_t^{QCD}:

$$\mu_i(N_t^{t\bar{t}}, N_t^B, N_t^{QCD}) = f_i^{t\bar{t}} N_t^{t\bar{t}} + f_i^B N_t^B + f_i^{QCD} N_t^{QCD} \tag{8}$$

where $f_i^{t\bar{t}}$, f_i^B, f_i^{QCD} are the contents of bins i of the normalized $t\bar{t}$, physics background, and multijet likelihood discriminant templates, respectively.

μ_i can be rewritten by

$$\mu_i(N_t^{t\bar{t}}, N_t^B, N_t^{QCD}) = f_i^{t\bar{t}} \cdot \sigma \cdot \mathcal{L} \cdot \mathcal{B}r \cdot \varepsilon + f_i^B N_t^B + f_i^{QCD} N_t^{QCD} \tag{9}$$

where σ is the $t\bar{t}$ cross section, $\mathcal{B}r \cdot \varepsilon$ is the total efficiency times branching ratio of $t\bar{t}$ and $\mathcal{L}$ is the integrated luminosity.

The second term of Eq. 7 is a poisson constraint on the observed number of events in the **Loose** but not **Tight** sample and effectively completes the incorporation of the Matrix Method in the likelihood. By introducing $N_{\ell-t} = N_\ell - N_t$ one makes sure that $N_{\ell-t}$ and N_t (implicitly present in the likelihood discriminant histogram) are indeed uncorrelated by construction.

The next step is to express $N_{\ell-t}$ in terms of $N_t^{t\bar{t}}$, N_t^B and N_t^{QCD}. The Matrix Method (Eq. 1) can be rewritten in the following way:

$$\begin{aligned} N_\ell &= N^{t\bar{t}} + N^B + N^{QCD} \\ N_t &= \varepsilon_{sig} N^{t\bar{t}} + \varepsilon_{sig} N^{B+} + \varepsilon_{QCD} N^{QCD} \end{aligned} \tag{10}$$

Introducing also the numbers of the individual components in the preselected events as $N_t^{t\bar{t}} = \varepsilon_{sig} N^{t\bar{t}}$, $N_t^B = \varepsilon_{sig} N^B$, and $N_t^{QCD} = \varepsilon_{QCD} N^{QCD}$, one obtains:

$$N_{\ell-t} = \frac{1-\varepsilon_{sig}}{\varepsilon_{sig}} N_t^{t\bar{t}} + \frac{1-\varepsilon_{sig}}{\varepsilon_{sig}} N_t^B + \frac{1-\varepsilon_{QCD}}{\varepsilon_{QCD}} N_t^{QCD} \tag{11}$$

Thus, the task is to minimize:

$$-\log L(N_t^{t\bar{t}}, N_t^B, N_t^{QCD}) = \sum_i -n_i^{obs} \log \mu_i + \mu_i - N_{\ell-t}^{obs} \log N_{\ell-t} + N_{\ell-t} \tag{12}$$

where, as already mentioned, μ_i and $N_{\ell-t}$ are functions of σ, N_t^B and N_t^{QCD} as given, respectively, by Eq. 8 and 11.

1. *W+jets and $t\bar{t}$ Contamination in the QCD-multijets Template*

The shape of the likelihood discriminant for the QCD-multijets background is taken from the "loose-tight" data sample, requiring the full preselection but inverting the tight lepton likelihood selection. Rewriting Eq. 11, one can see that the "loose-tight" QCD-multijets ($N_{\ell-t}$) data sample is contaminated with W+jets and $t\bar{t}$:

$$N_{\ell-t} = \frac{1-\varepsilon_{sig}}{\varepsilon_{sig}}(\sigma \cdot \mathcal{L} \cdot \mathcal{B}r \cdot \varepsilon) + \frac{1-\varepsilon_{sig}}{\varepsilon_{sig}} N_t^B + N_{\ell-t}^{QCD} \tag{13}$$

The contamination of the QCD template is taken into account by using the corrected expected number of events in each bin of the likelihood discriminant

$$\mu_i(N_t^{t\bar{t}}, N_t^B, N_t^{QCD}) = (f_i^{t\bar{t}} \cdot \sigma \cdot \mathcal{L} \cdot \mathcal{B}r \cdot \varepsilon + f_i^B N_t^B) \cdot (1 - \frac{\varepsilon_{QCD}}{1-\varepsilon_{QCD}} \frac{1-\varepsilon_{sig}}{\varepsilon_{sig}}) + f_i^{QCD}(N_t^{QCD} + \frac{\varepsilon_{QCD}}{1-\varepsilon_{QCD}} \frac{1-\varepsilon_{sig}}{\varepsilon_{sig}}((\sigma \cdot \mathcal{L} \cdot \mathcal{B}r \cdot \varepsilon) + N_t^B)) \tag{14}$$

instead of the one of equation (8).

Finally we find the cross section by minimizing $\sum_i(-\log L_i)$ with respect to σ, N_t^B and N_t^{QCD}. The sum runs over the four channels defined by the lepton flavor (e, μ) and the jet multiplicity (3, $\geq$4).

VIII. SYSTEMATIC UNCERTAINTIES

The systematic uncertainties can be subdivided into uncertainties on the preselection efficiency and uncertainties on the estimated number of selected $t\bar{t}$ signal events from the Maximum Likelihood Fit described in VII. Systematic uncertainties (observed) on the cross section are evaluated by varying the source of the systematic uncertainty, rederiving the likelihood templates for the $t\bar{t}$ signal, the background and preselection efficiency and repeating the likelihood fit to the data.

We assign the standard 6.1% uncertainty to the integrated luminosity measurement [40].

A. Uncertainties on the Preselection Efficiency

The $t\bar{t}$ preselection efficiency as well as the preselection efficiencies for other backgrounds are determined by applying the full preselection on Monte Carlo events.

Other sources of systematic uncertainties are differences between data and Monte Carlo in terms of object reconstruction efficiency.

A detailed description of the systematic uncertainties contributing to the preselection efficiency uncertainty and methods used to evaluate them is given in Section IX of Refs. [3].

Primary Vertex Scale Factor This systematic uncertainty arises from the difference between data and MC for the selection of vertices with $|Z| < 60$ cm with ≥ 3 tracks and $\Delta|PV - PV_{Lepton}| < 1$ cm. It is and found to be 1.5% [36].

Vertex Z position simulation Based on the study "The longitudinal shape of the luminous region at D0" [42] and derived the uncertainty coming solely from the inaccurate vertex z position simulation to be 1.6% for p17 data set.

Luminosity profile in data and MC The luminosity profiles of the MC and data samples are somewhat different. We assign an uncertainty equal to the difference between the result obtained with the default MC luminosity profile and the result obtained with the MC reweighted to match the luminosity profile of the data sample.

Parton distribution functions The computed acceptance for $t\bar{t}$ events depends on the parton distribution functions used. We apply an uncertainty that corresponds to the shift observed when the parton momenta are reweighted from the CTEQ6L1 pdf set to the CTEQ6.1M sets.[33]

Electron identification efficiency According to the study from di-lepton cross section measurement group, this systematic uncertainty is 2.5%. 1.3% is from jet multiplicity dependence [33] and 2.3% [41] from dependence on other quantities.

Muon identification efficiency This systematic uncertainty is estimated by the muon ID group (0.7%) and includes uncertainties from the tag and probe method used to measure efficiencies, background subtraction and binning. [43]

Muon tracking efficiency This systematic uncertainty is estimated by the muon ID group (0.7%) and includes uncertainties from the tag and probe method used to measure efficiencies, background subtraction, binning, luminosity, time bias and averaging over ϕ. [43]

Muon isolation efficiency We estimate this uncertainty from the dependence of the isolation scale factor on the number of jets to be 2%.

Trigger Efficiency The trigger efficiency as a function of p_{T} for each object in a MC event is shifted up and down by one standard deviation and the weight of the event recalculated. This shift is taken as an overall constant systematic error on the MC acceptance.

Jet energy resolution The uncertainty on the jet energy resolution in data is already included in the systematic uncertainty due to the jet energy scale. The energy of jets in Monte Carlo is smeared to the jet energy resolution of data. The jet energy resolution in Monte Carlo has an uncertainty which is not taken into account in the jet energy scale. To account for this, the parameters of the jet energy smearing are varied by the size of the uncertainty on the jet energy resolution parameters in Monte Carlo.

Jet Reconstruction This is the systematic uncertainty on the correction of the jet reconstruction.

Jet Identification Efficiency This is the systematic uncertainty on identification efficiency in the simulation.

b **fragmentation** The DØ MC simulation uses the default *b*-quark fragmentation provided by PYTHIA. We quote the difference between this default fragmentation and the fragmentation functions tuned to LEP data [44] as systematic uncertainty. The LEP fragmentation was implemented by reweighting the events accordingly.

MC Factorization scale The factorization scale is estimated by calculating the fitted number of $t\bar{t}$ events on a W+jets background Monte Carlo sample generated with $Q^2 =< p_{T_j} >^2$ instead of the default scale $Q^2 = M_W^2 + \sum p_{T_j}^2$. Changing the factorization scale from the default $Q^2 = M_W^2 + \sum p_{T_j}^2$ to $Q^2 =< p_{T_j} >^2$ leads to softer p_T spectra, whereas other tested factorization scales lead to harder p_T spectra. Since the distributions for $Q^2 = M_W^2 + \sum p_{T_j}^2$ are found to be well centered between the other choices, it is a good approximation to symmetrize the one-sided error determined from the choice of $Q^2 =< p_{T_j} >^2$ as factorization scale [45]. We have carried out the study for W+light jets and the effect of scale variation is completely negligible. This is a feature of the matched ALPGEN which compensates the difference.

Uncertainty on ε_{sig} and ε_{QCD} The uncertainty on the number of W+jets and QCD events per exclusive jet multiplicity after preselection obtained from the Matrix Method is obtained by varying ε_{sig} and ε_{bkg} by one standard deviation. The results of the two variations are added in quadrature. The uncertainties are assumed to be totally uncorrelated between the channels.

B. Ensemble Test

Expected systematics are obtained by the likelihood fit with varying the source of the systematic uncertainty, rederiving the likelihood templates for the $t\bar{t}$ signal, the background and preselection efficiency to the fake data set and finding $\Delta\sigma$ with the value Eq.(15) where the fake data set (ensemble) constructed based on the default templates of $t\bar{t}$, backgrounds and multijet for the cross section measurements Eq.(15) with allowing for Poisson fluctuations in the fraction of each template for 1000 times. The mean of the distribution of the $\Delta\sigma$ is an estimate of the systematic uncertainty. We used expected systematic uncertainty since observed systematic uncertainty has limited statistics. Tables 15- 17 show the summaries of systematics uncertainties $\Delta\sigma_{t\bar{t}}$ (pb).

TABLE 15: Summary of systematic uncertainties $\Delta\sigma_{t\bar{t}}$ (pb) for e+jets.

Source	observed	expected	e+jets
Primary vertex	$+\,0.13-0.12$		$+\,0.13-0.12$
Electron identification	$+\,0.16-0.15$		$+\,0.16-0.15$
Muon identification	$+\,0.00-0.00$		$+\,0.00-0.00$
Trigger	$+\,0.08-0.04$		$+\,0.08-0.04$
epsSIG	$+\,0.03-0.03$		$+\,0.03-0.03$
epsQCD	$+\,0.15-0.15$		$+\,0.15-0.15$
PDF	$+\,0.00-0.01$		$+\,0.00-0.01$
Jet energy calibration	$+\,0.35-0.06$	$+\,0.31-0.00$	$+\,0.31-0.00$
Jet identification	$+\,0.12-0.12$	$+\,0.12-0.12$	$+\,0.12-0.12$
Jet resolution	$+\,0.00-0.15$	$+\,0.00-0.13$	$+\,0.00-0.13$
B Fragmentation	$+\,0.18-0.00$	$+\,0.13-0.00$	$+\,0.13-0.00$
Factorization	$+\,0.00-0.00$	$+\,0.00-0.13$	$+\,0.00-0.13$
Luminosity Profile	$+\,0.16-0.00$	$+\,0.15-0.00$	$+\,0.15-0.00$
Template Modeling		$+\,0.21-0.21$	$+\,0.21-0.21$
Total			$+\,0.52-0.40$

TABLE 16: Summary of systematic uncertainties $\Delta\sigma_{t\bar{t}}$ (pb) for μ+jets.

Source	observed	expected	μ+jets
Primary vertex	$+\,0.14-0.14$		$+\,0.14-0.14$
Electron identification	$+\,0.00-0.00$		$+\,0.00-0.00$
Muon identification	$+\,0.17-0.16$		$+\,0.17-0.16$
Trigger	$+\,0.20-0.17$		$+\,0.20-0.17$
epsSIG	$+\,0.07-0.07$		$+\,0.07-0.07$
epsQCD	$+\,0.06-0.05$		$+\,0.06-0.05$
PDF	$+\,0.00-0.01$		$+\,0.00-0.01$
Jet energy calibration	$+\,0.71-0.36$	$+\,0.71-0.41$	$+\,0.71-0.36$
Jet identification	$+\,0.13-0.13$	$+\,0.12-0.12$	$+\,0.12-0.12$
Jet resolution	$+\,0.00-0.12$	$+\,0.03-0.08$	$+\,0.03-0.08$
B Fragmentation	$+\,0.09-0.00$	$+\,0.10-0.00$	$+\,0.10-0.00$
Factorization	$+\,0.01-0.01$	$+\,0.03-0.08$	$+\,0.03-0.08$
Luminosity Profile	$+\,0.19-0.00$	$+\,0.18-0.00$	$+\,0.18-0.00$
Template Modeling		$+\,0.21-0.21$	$+\,0.21-0.21$
Total			$+\,0.84-0.57$

TABLE 17: Summary of systematic uncertainties $\Delta\sigma_{t\bar{t}}$ (pb) for l+jets.

Source	observed	expected	l+jets
Primary vertex	$+\,0.13-0.13$		$+\,0.13-0.13$
Electron identification	$+\,0.10-0.10$		$+\,0.10-0.10$
Muon identification	$+\,0.06-0.06$		$+\,0.06-0.06$
Trigger	$+\,0.12-0.09$		$+\,0.12-0.09$
epsSIG	$+\,0.05-0.04$		$+\,0.05-0.04$
epsQCD	$+\,0.11-0.10$		$+\,0.11-0.10$
PDF	$+\,0.00-0.01$		$+\,0.00-0.01$
Jet energy calibration	$+\,0.50-0.19$	$+\,0.47-0.16$	$+\,0.47-0.16$
Jet identification	$+\,0.12-0.12$	$+\,0.12-0.12$	$+\,0.12-0.12$
Jet resolution	$+\,0.00-0.14$	$+\,0.00-0.11$	$+\,0.00-0.11$
B Fragmentation	$+\,0.14-0.00$	$+\,0.12-0.00$	$+\,0.12-0.00$
Factorization	$+\,0.00-0.00$	$+\,0.00-0.11$	$+\,0.00-0.11$
Luminosity Profile	$+\,0.17-0.00$	$+\,0.16-0.00$	$+\,0.16-0.00$
Template Modeling		$+\,0.15-0.15$	$+\,0.15-0.15$
Total			$+\,0.60-0.37$

IX. RESULT

The result of the likelihood fit is shown in Fig. 19. The inputs and results for the likelihood fit are summarised in Table IX.

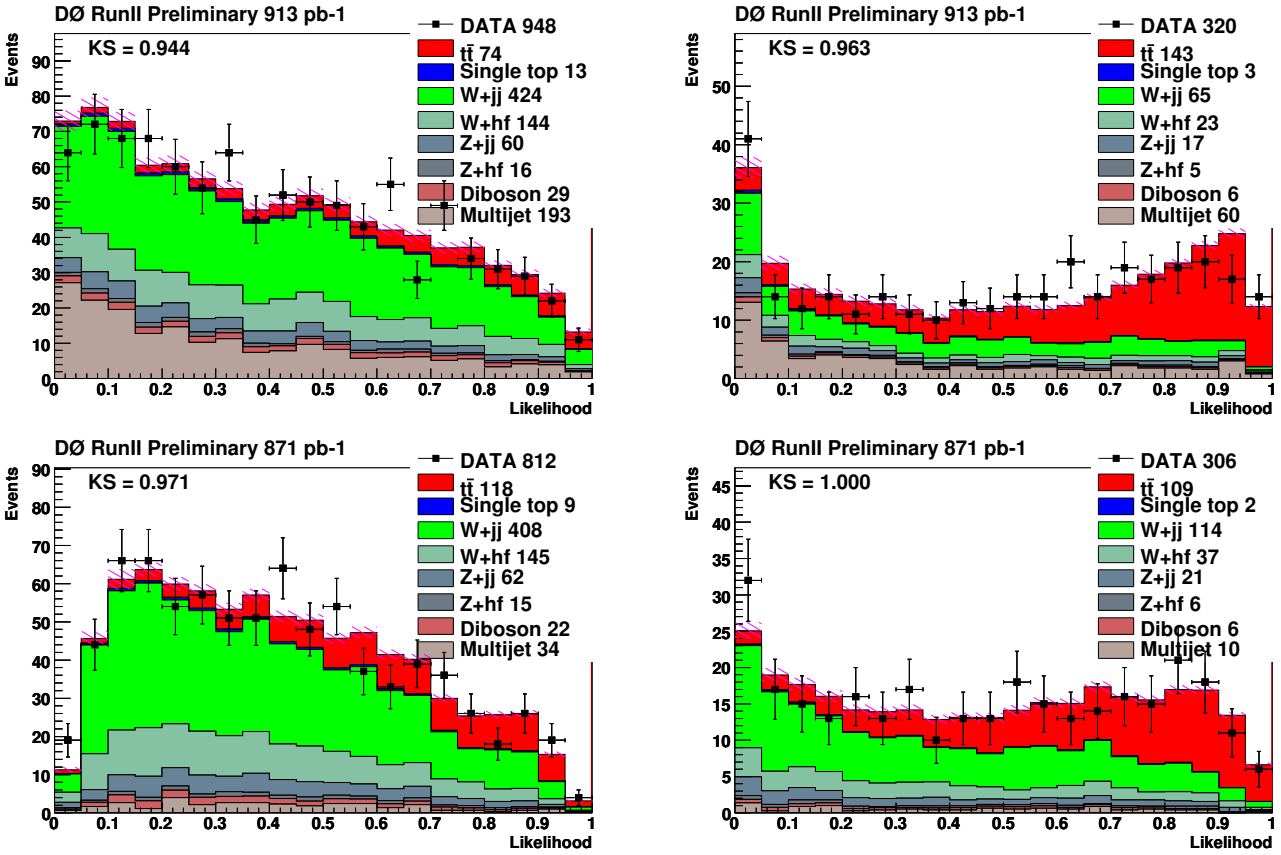

FIG. 19: Likelihood discriminant distribution for data overlaid with the result from the fit of $t\bar{t}$, backgrounds and QCD-multijets for e+jets =3 (top left), e+jets $\geq$4 (top right), μ+jets =3(bottom left) and μ+jets $\geq$4(bottom right).

	N_l	N_t	$\mathcal{B}r$	$\mathcal{L}$ (pb^{-1})	ε	ε_{sig}	ε_{QCD}	N_t^{tt}
e+jets =3	1885	948	0.17	912.5	0.02	0.85	0.2	$74.4\ ^{+39.6}_{-37.6}$
e+jets $\geq$4	618	320	0.17	912.5	0.021	0.84	0.2	$142.6\ ^{+24.9}_{-23.9}$
μ+jets =3	1015	812	0.17	871.3	0.015	0.87	0.27	$118.3\ ^{+35.5}_{-34.2}$
μ+jets $\geq$4	388	306	0.17	871.3	0.018	0.85	0.27	$109.5\ ^{+22.8}_{-21.8}$

TABLE 18: Inputs and results for the Likelihood Discriminant fit for the e+jets =3, e+jets $\geq$4, μ+jets =3 and μ+jets $\geq$4.

The result of the $t\bar{t}$ production cross-section in the l+jets channel at $\sqrt{s}$ =1.96 TeV for a top mass of 175 GeV yields with systematic study in Section VIII:

$$e+\text{jets}\ :\quad \sigma_{p\bar{p}\to t\bar{t}+X} = 6.22^{+1.04}_{-1.00}\,(\text{stat})\,^{+0.52}_{-0.40}\,(\text{syst})\ \pm 0.38\,(\mathcal{L})\ \text{pb}$$

$$\mu+\text{jets}\ :\quad \sigma_{p\bar{p}\to t\bar{t}+X} = 7.06^{+1.21}_{-1.17}\,(\text{stat})\,^{+0.84}_{-0.57}\,(\text{syst})\ \pm 0.43\,(\mathcal{L})\ \text{pb}$$

$$l+\text{jets}\ :\quad \sigma_{p\bar{p}\to t\bar{t}+X} = 6.59^{+0.78}_{-0.77}\,(\text{stat})\,^{+0.60}_{-0.37}\,(\text{syst})\ \pm 0.40\,(\mathcal{L})\ \text{pb}$$

APPENDIX A: CONTROL PLOTS FOR 1 JET BIN CHANNEL

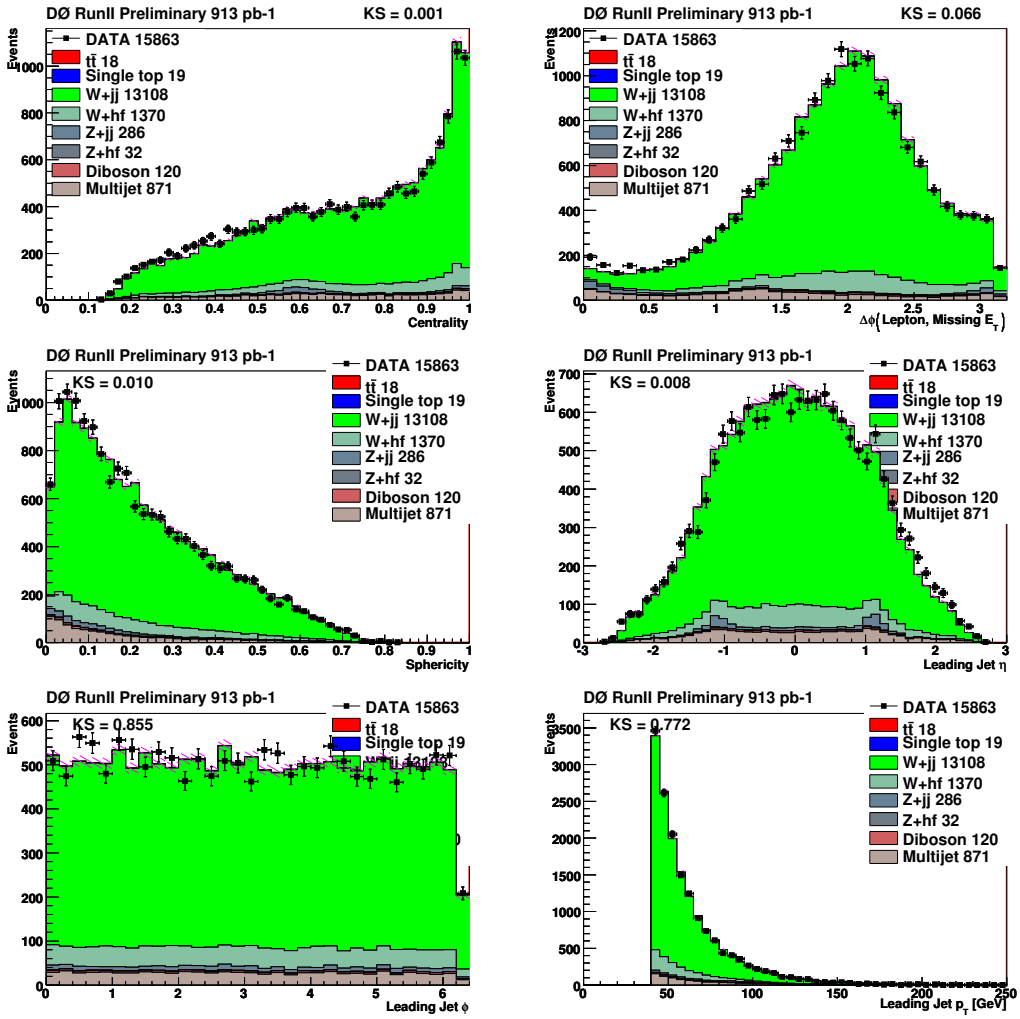

FIG. 20: *1-jet-bin* : Likelihood discriminant input distributions for the data overlaid with the result from the fit of $t\bar{t}$ (6.8 pb), backgrounds and QCD-multijets for the e+jets analysis.

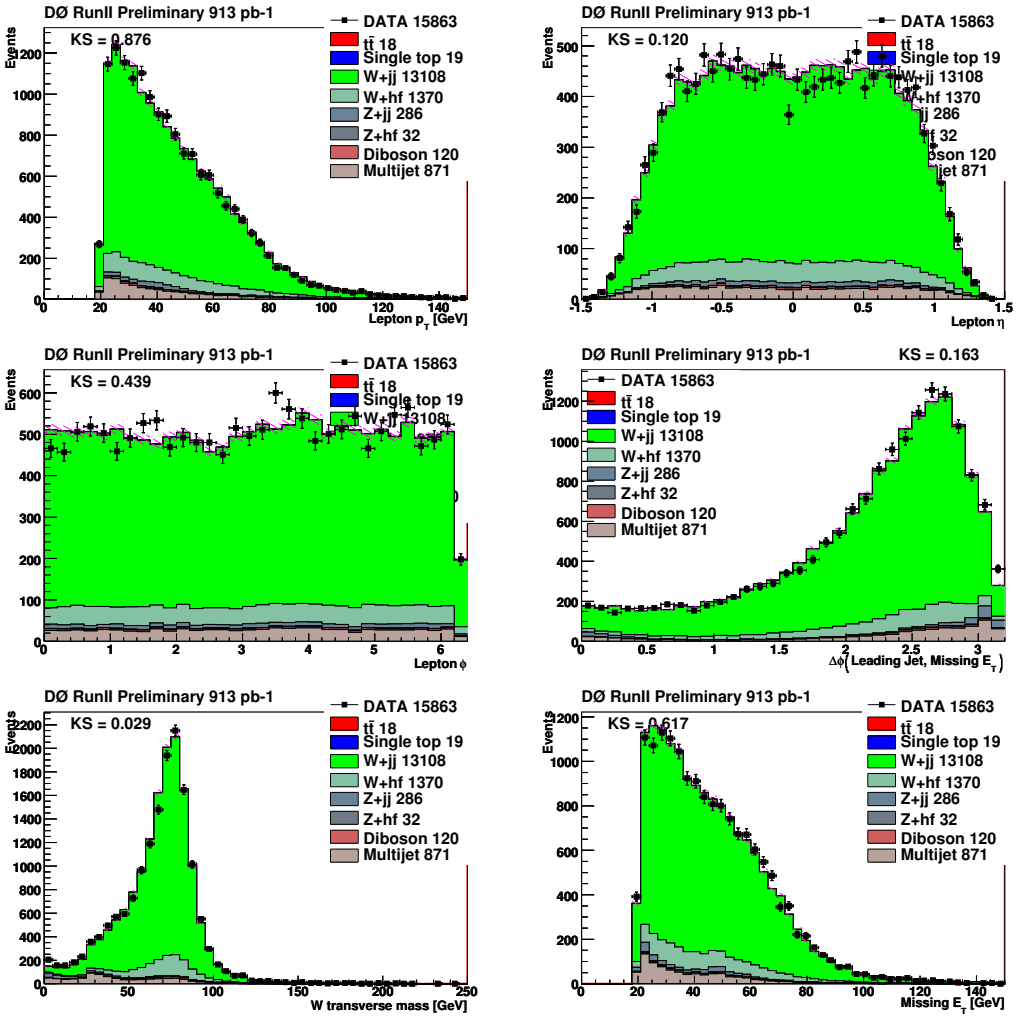

FIG. 21: *1-jet-bin* : Various distributions for the data overlaid with the result from the fit of $t\bar{t}$ (6.8 pb), backgrounds and QCD-multijets for the e+jets analysis.

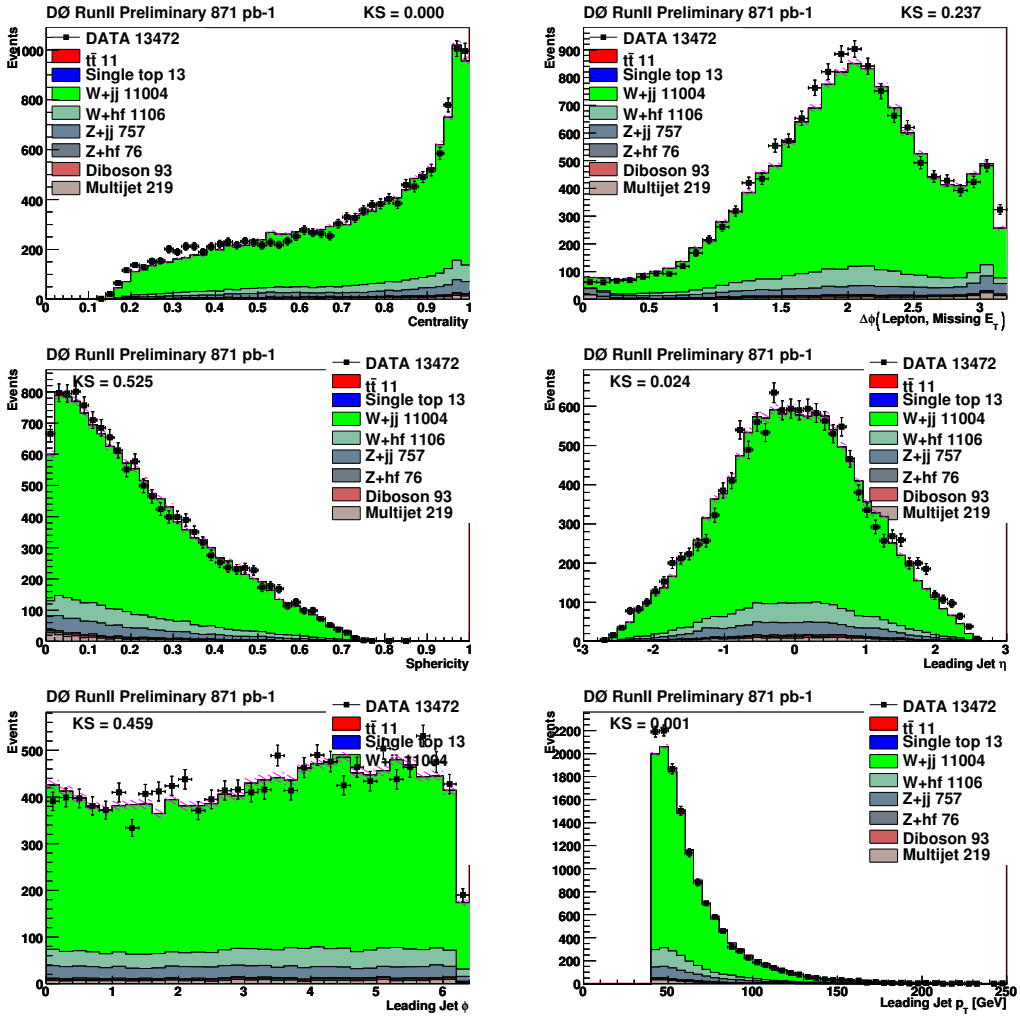

FIG. 22: *1-jet-bin* : Likelihood discriminant input distributions for the data overlaid with the result from the fit of $t\bar{t}$ (6.8 pb), backgrounds and QCD-multijets for the μ+jets analysis.

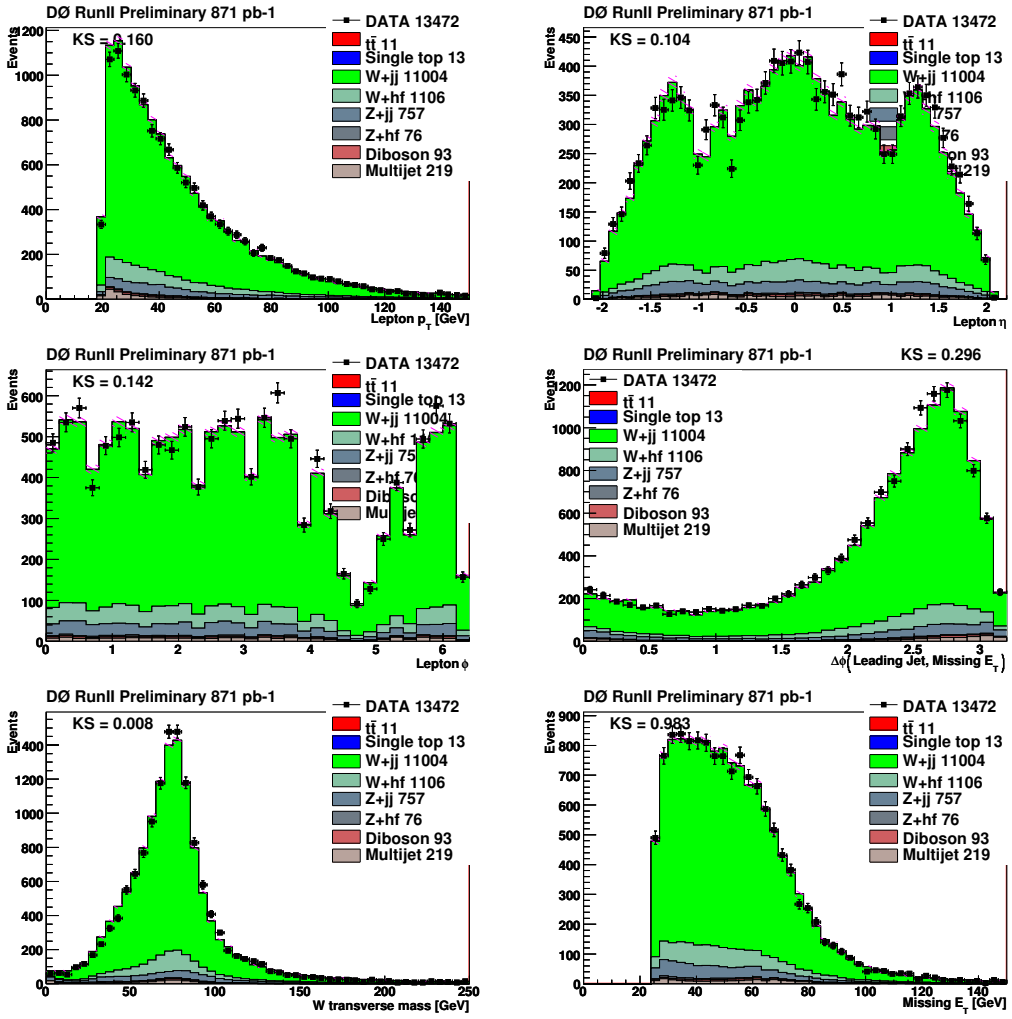

FIG. 23: *1-jet-bin* : Various distributions for the data overlaid with the result from the fit of $t\bar{t}$ (6.8 pb), backgrounds and QCD-multijets for the μ+jets analysis.

APPENDIX B: CONTROL PLOTS FOR 2 JET BIN CHANNEL

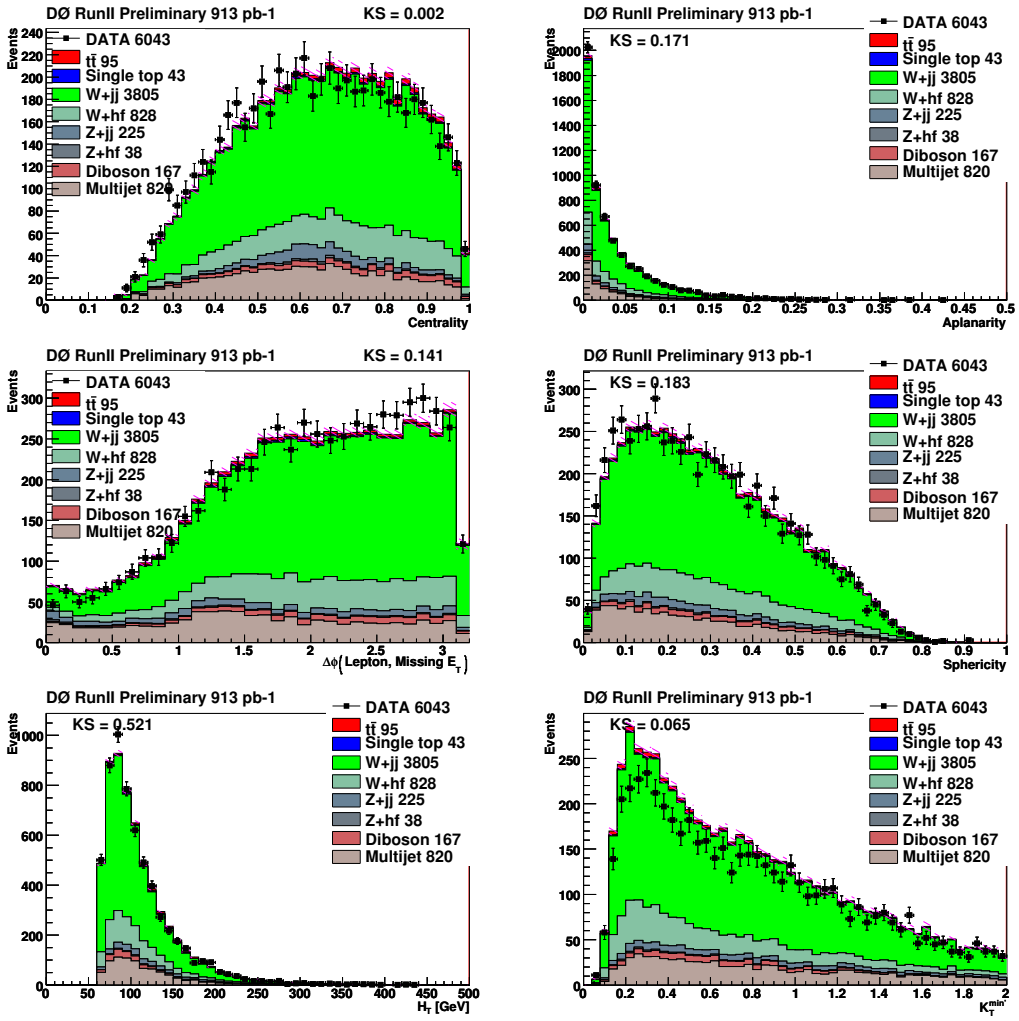

FIG. 24: *2-jet-bin* : Likelihood discriminant input distributions for the data overlaid with the result from the fit of $t\bar{t}$ (6.8 pb), backgrounds and QCD-multijets for the e+jets analysis.

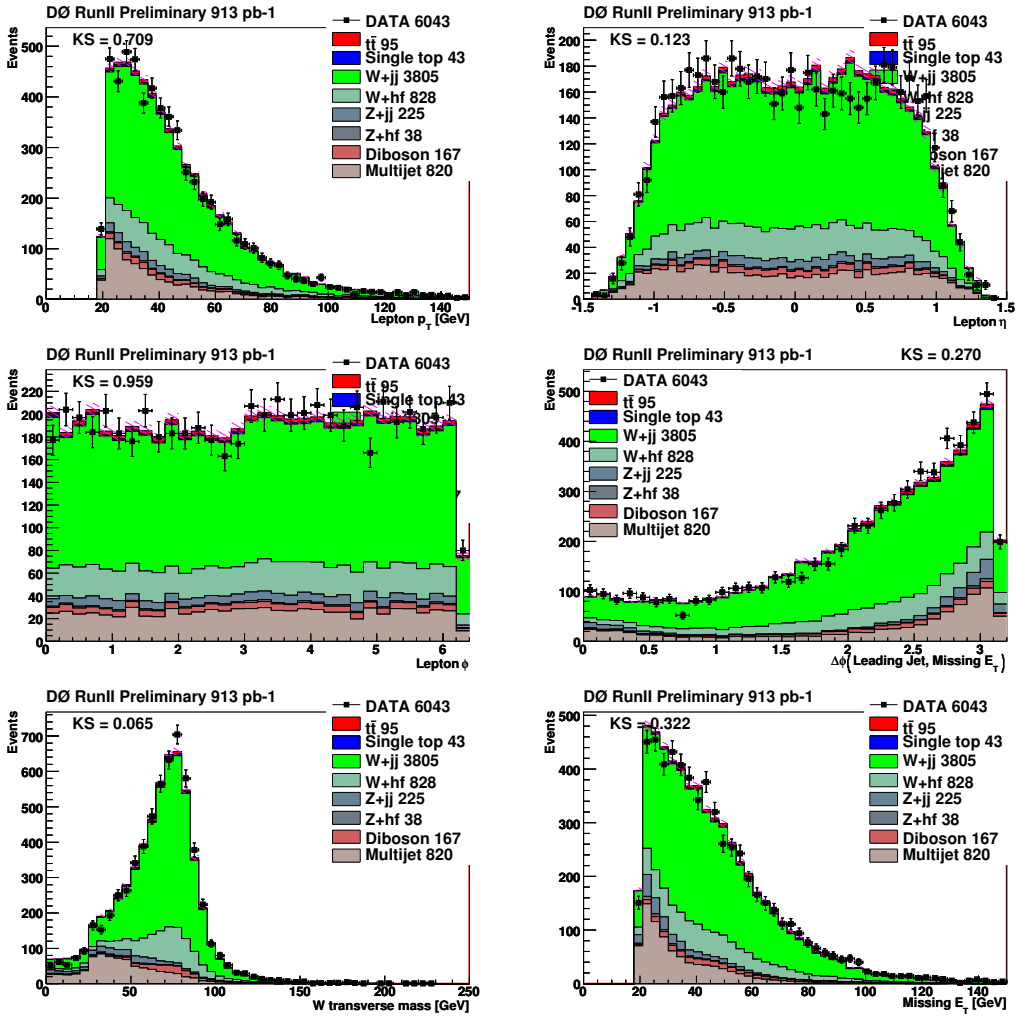

FIG. 25: *2-jet-bin* : Various distributions for the data overlaid with the result from the fit of $t\bar{t}$ (6.8 pb), backgrounds and QCD-multijets for the e+jets analysis.

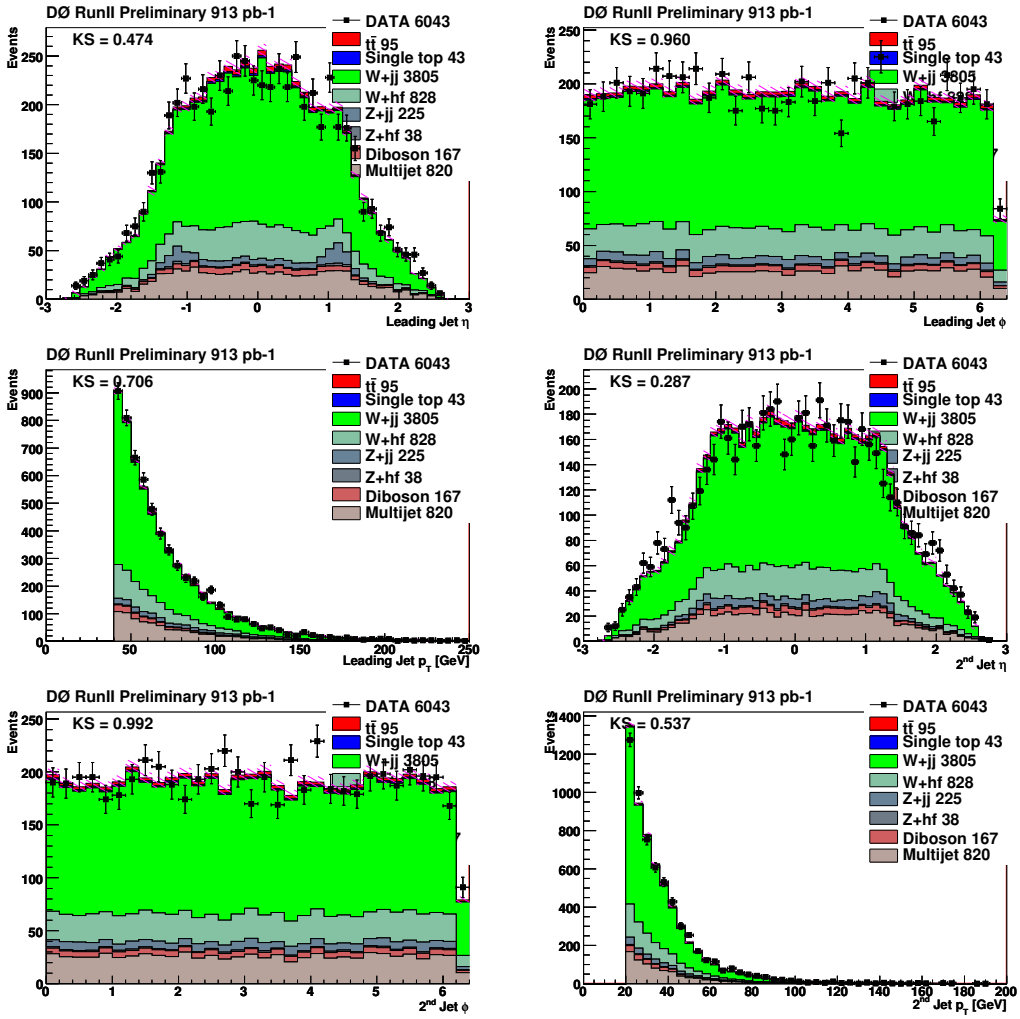

FIG. 26: *2-jet-bin* : Various distributions for the data overlaid with the result from the fit of $t\bar{t}$ (6.8 pb), backgrounds and QCD-multijets for the e+jets analysis.

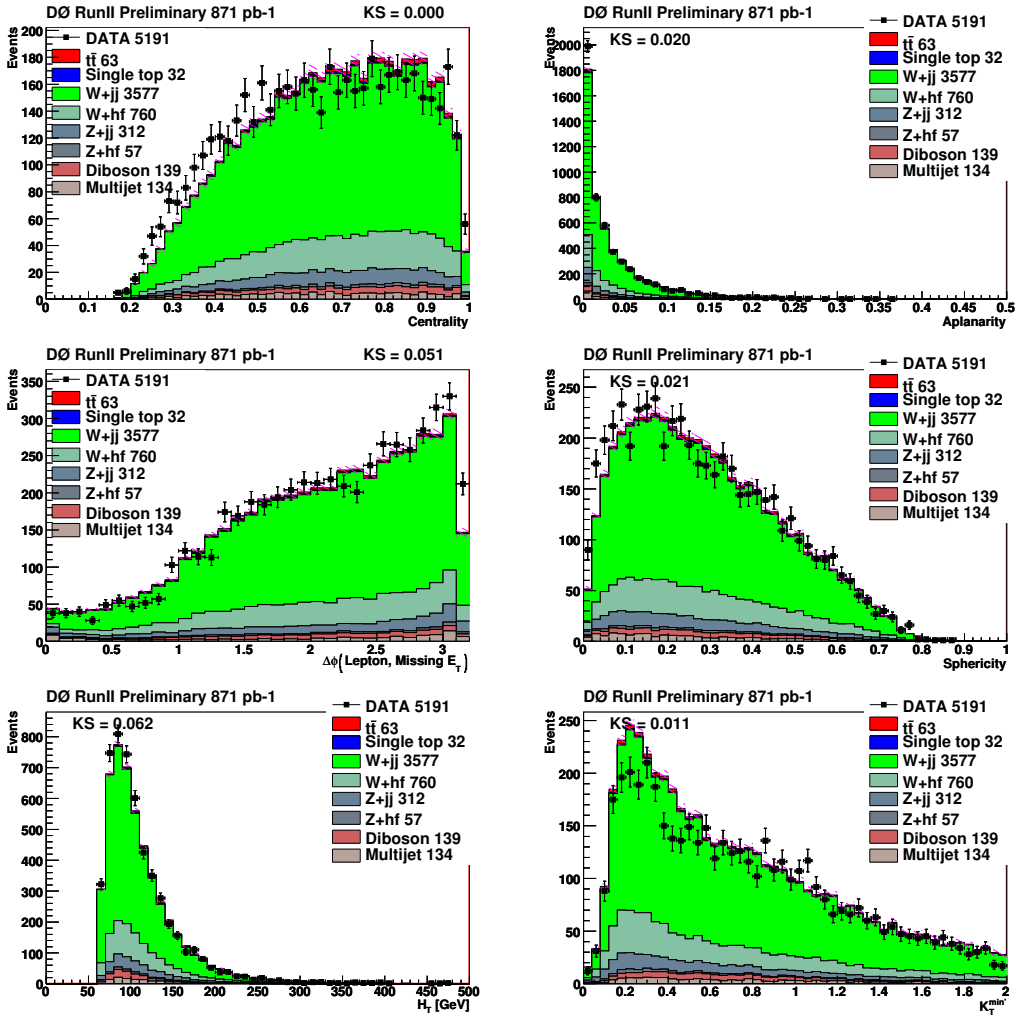

FIG. 27: *2-jet-bin* : Likelihood discriminant input distributions for the data overlaid with the result from the fit of $t\bar{t}$ (6.8 pb), backgrounds and QCD-multijets for the μ+jets analysis.

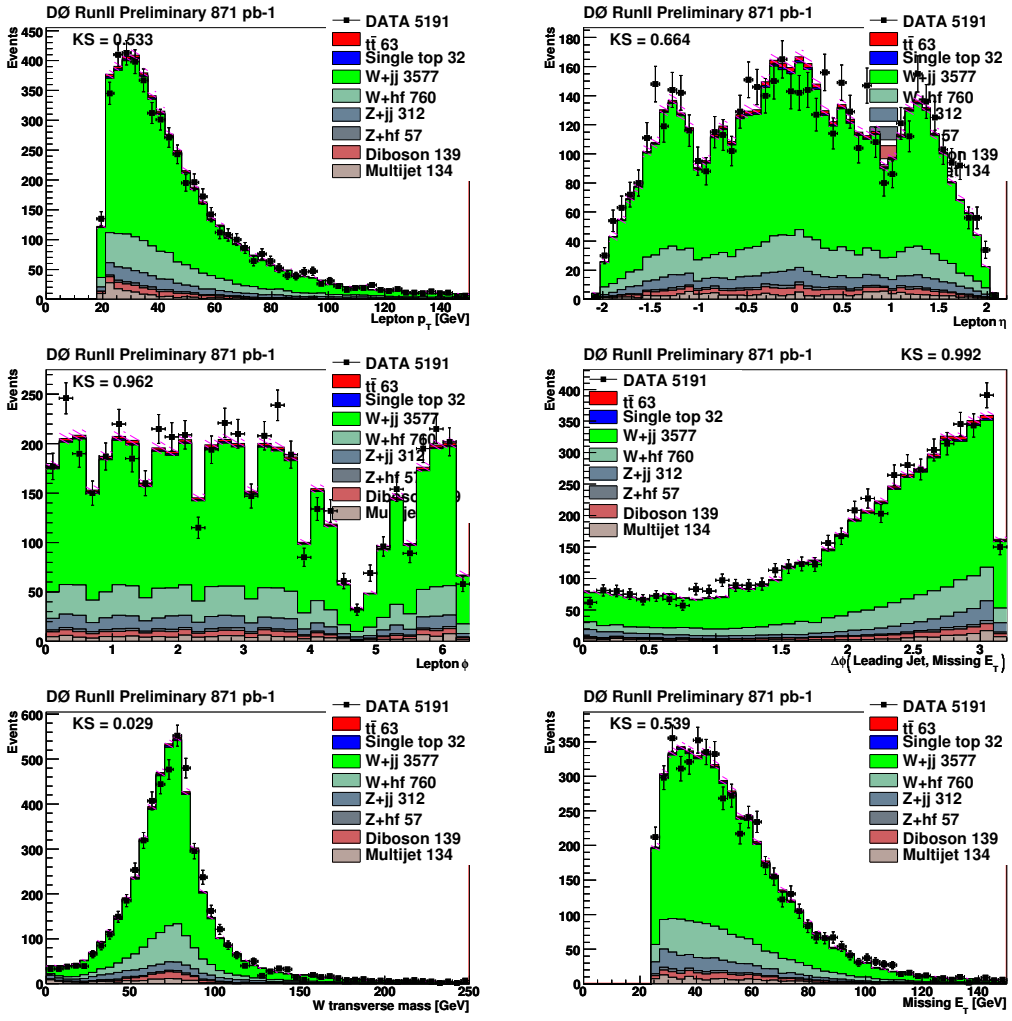

FIG. 28: *2-jet-bin* : Various distributions for the data overlaid with the result from the fit of $t\bar{t}$ (6.8 pb), backgrounds and QCD-multijets for the μ+jets analysis.

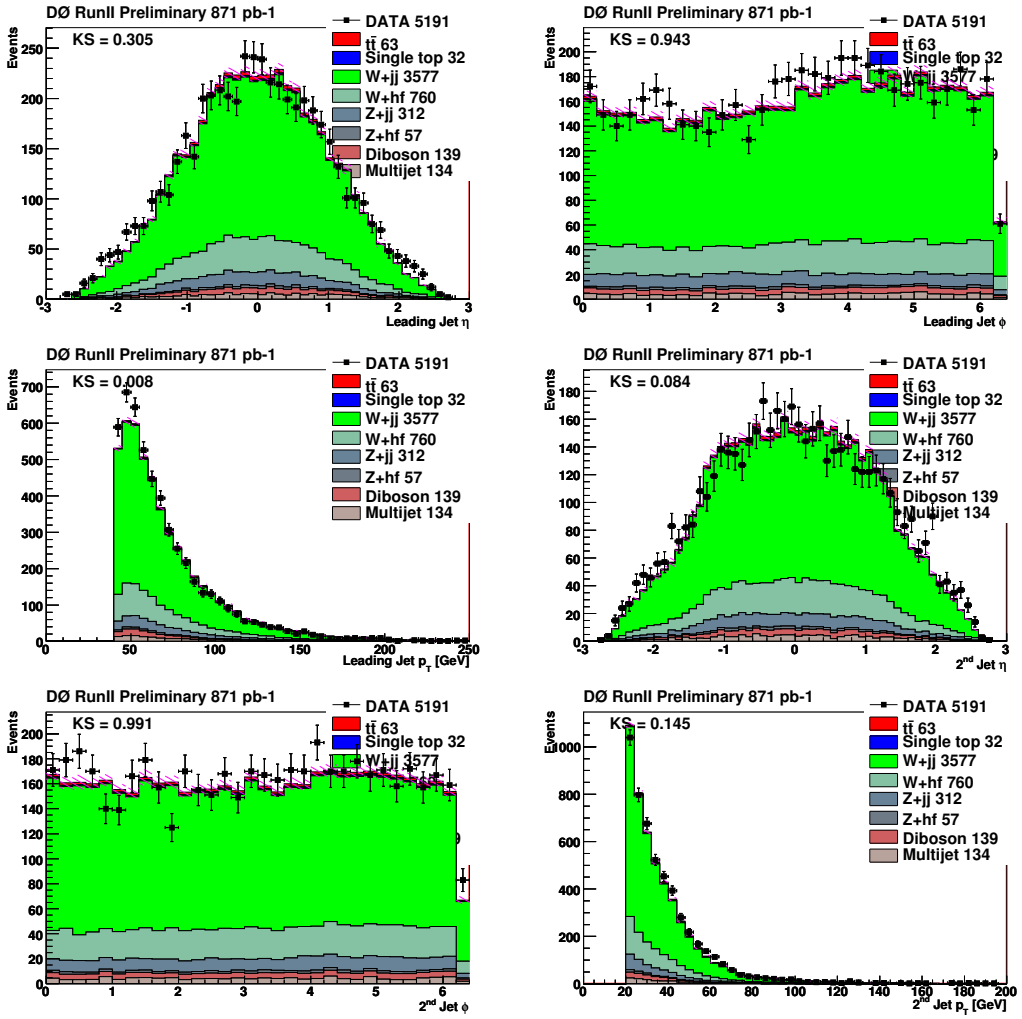

FIG. 29: *2-jet-bin* : Various distributions for the data overlaid with the result from the fit of $t\bar{t}$ (6.8 pb), backgrounds and QCD-multijets for the μ+jets analysis.

APPENDIX C: CONTROL PLOTS FOR 3 JET BIN CHANNEL

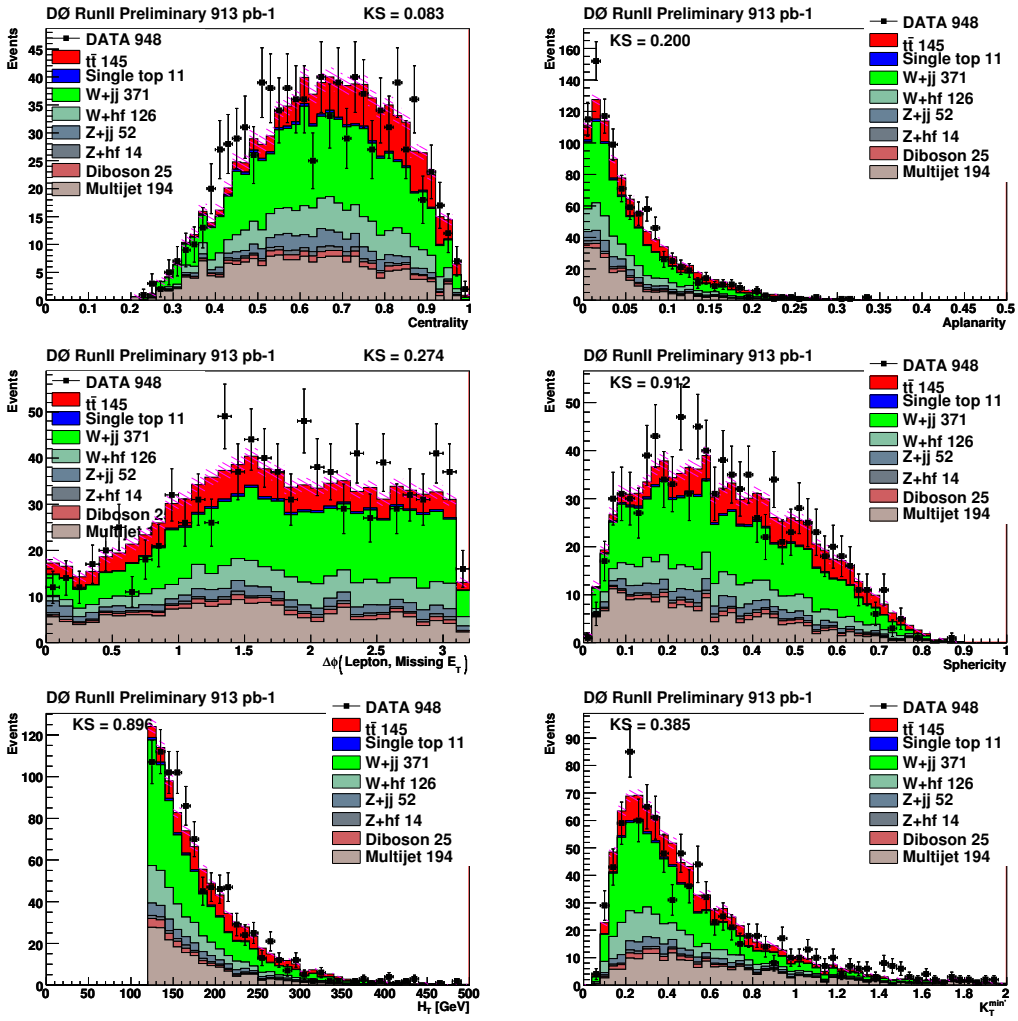

FIG. 30: *3-jet-bin* : Likelihood discriminant input distributions for the data overlaid with the result from the fit of $t\bar{t}$ (6.8 pb), backgrounds and QCD-multijets for the e+jets analysis.

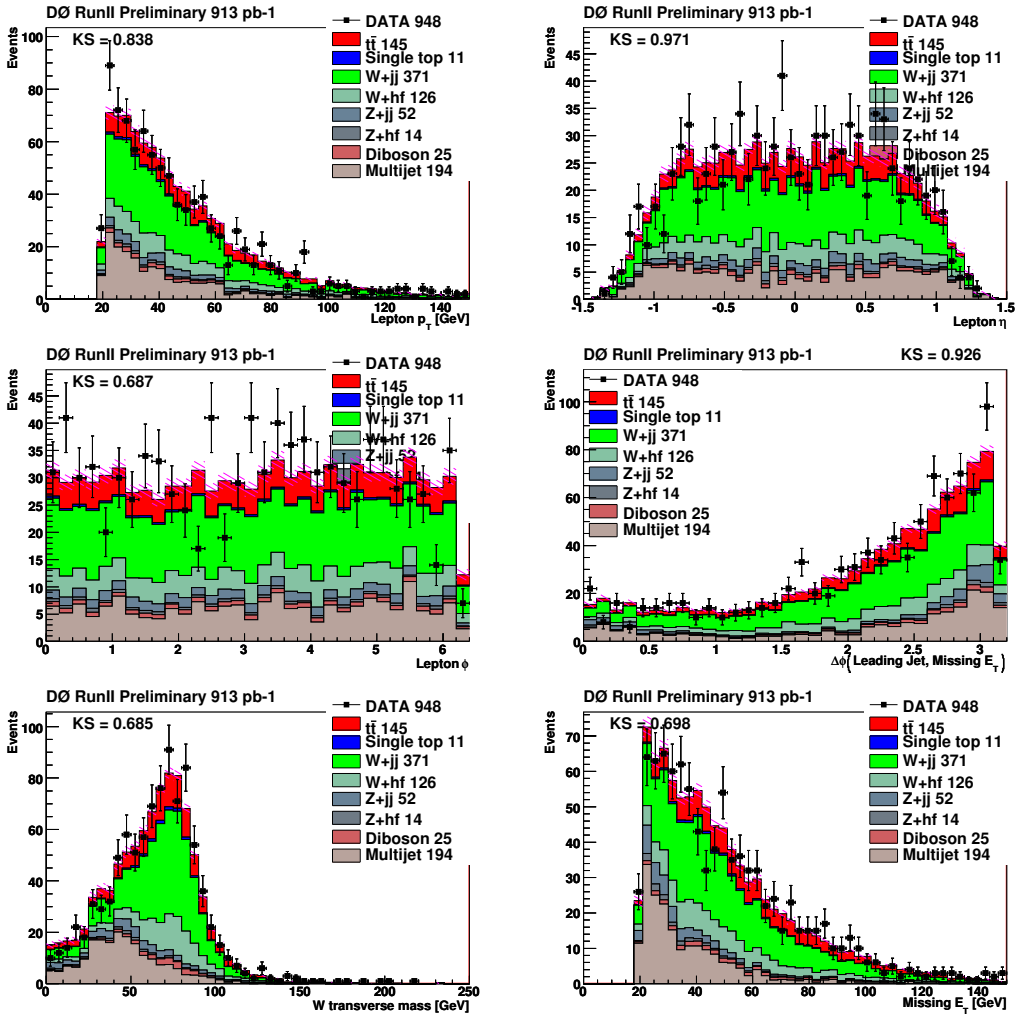

FIG. 31: *3-jet-bin* : Various distributions for the data overlaid with the result from the fit of $t\bar{t}$ (6.8 pb), backgrounds and QCD-multijets for the e+jets analysis.

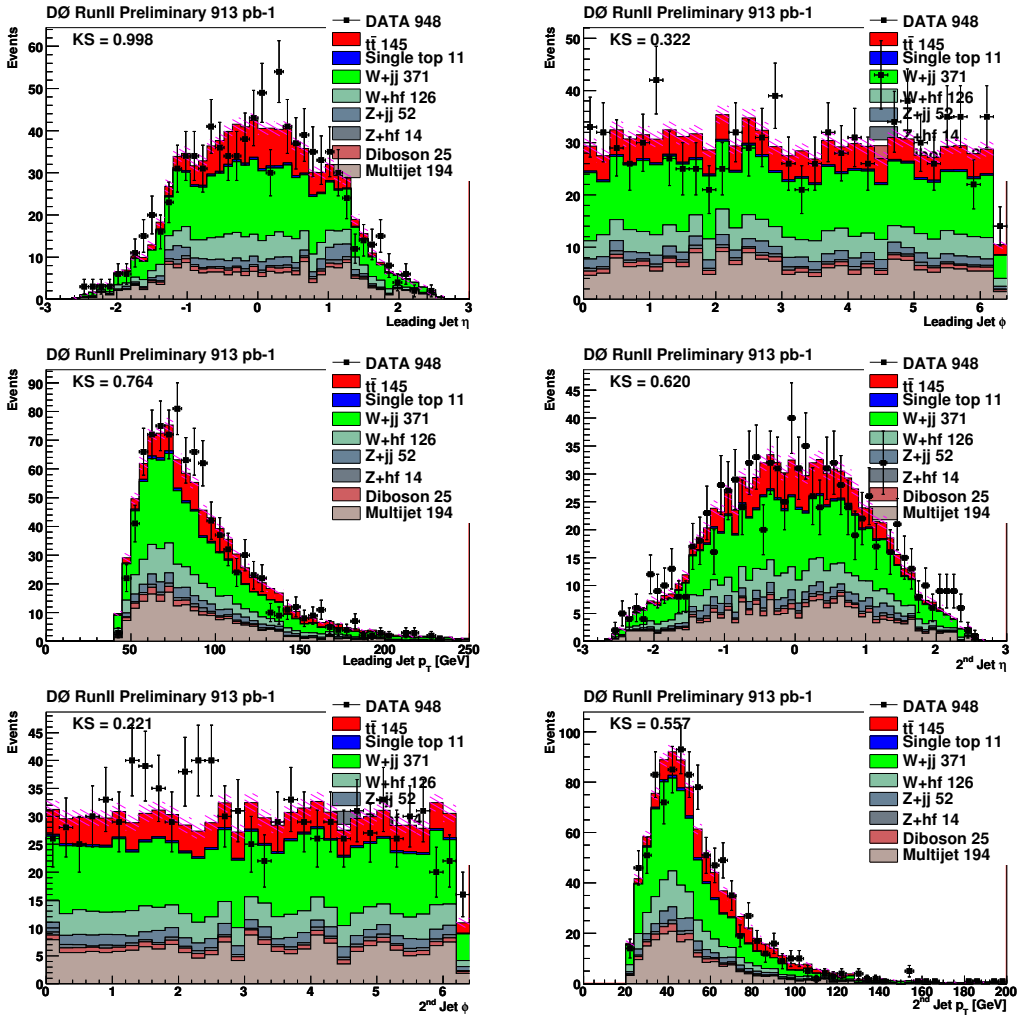

FIG. 32: *3-jet-bin* : Various distributions for the data overlaid with the result from the fit of $t\bar{t}$ (6.8 pb), backgrounds and QCD-multijets for the e+jets analysis.

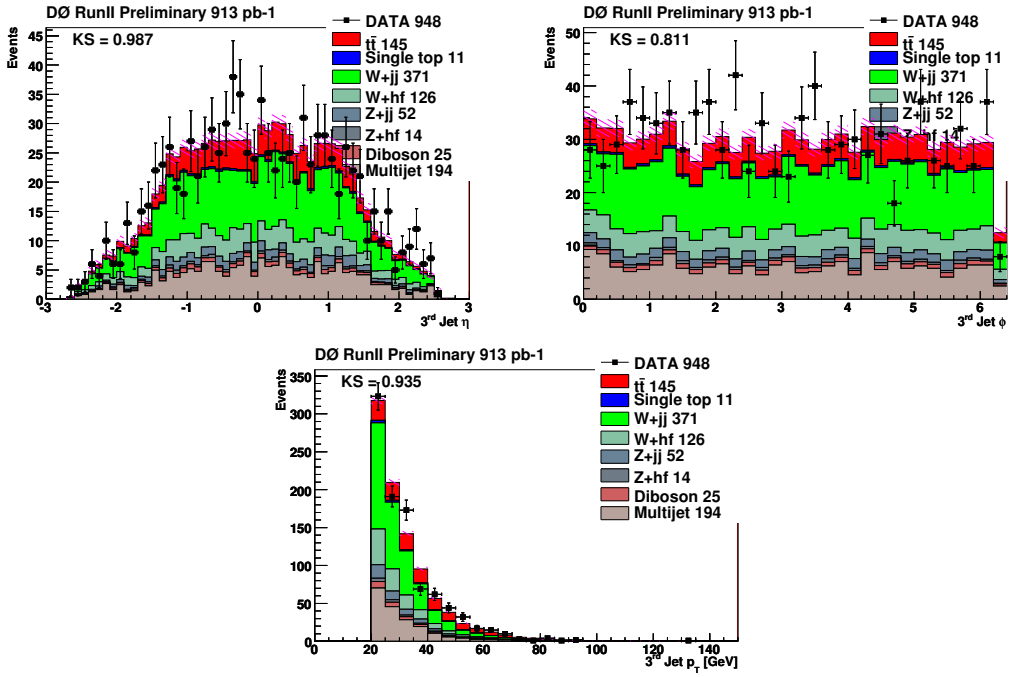

FIG. 33: *3-jet-bin* : Various distributions for the data overlaid with the result from the fit of $t\bar{t}$ (6.8 pb), backgrounds and QCD-multijets for the e+jets analysis.

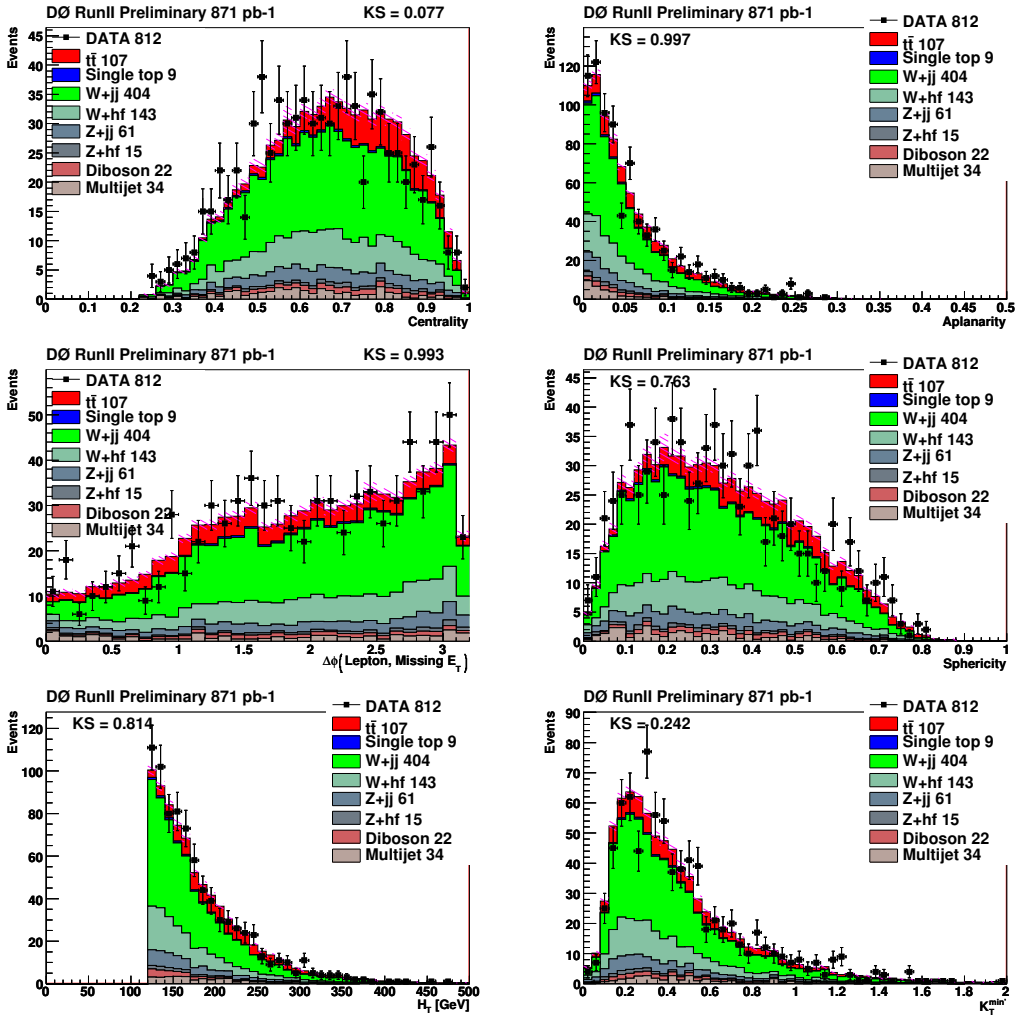

FIG. 34: *3-jet-bin* : Likelihood discriminant input distributions for the data overlaid with the result from the fit of $t\bar{t}$ (6.8 pb), backgrounds and QCD-multijets for the μ+jets analysis.

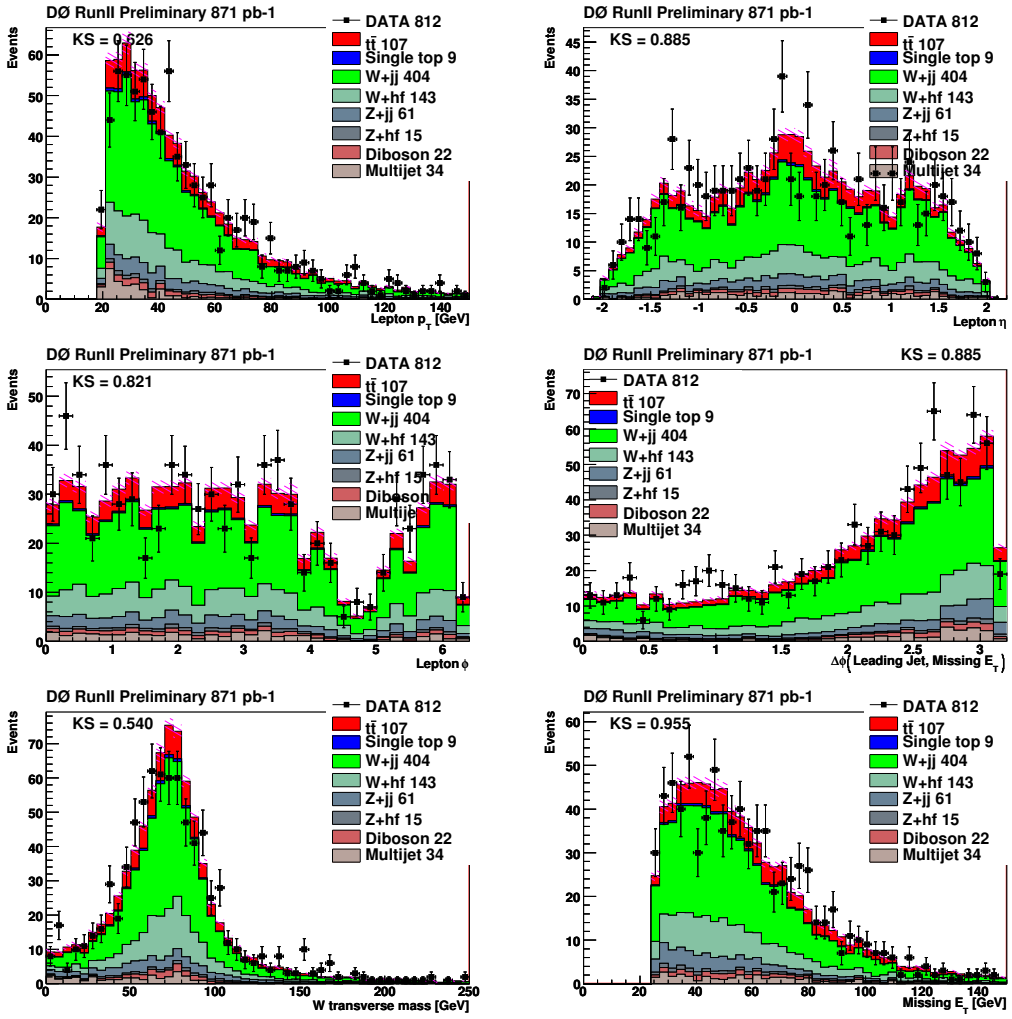

FIG. 35: *3-jet-bin* : Various distributions for the data overlaid with the result from the fit of $t\bar{t}$ (6.8 pb), backgrounds and QCD-multijets for the μ+jets analysis.

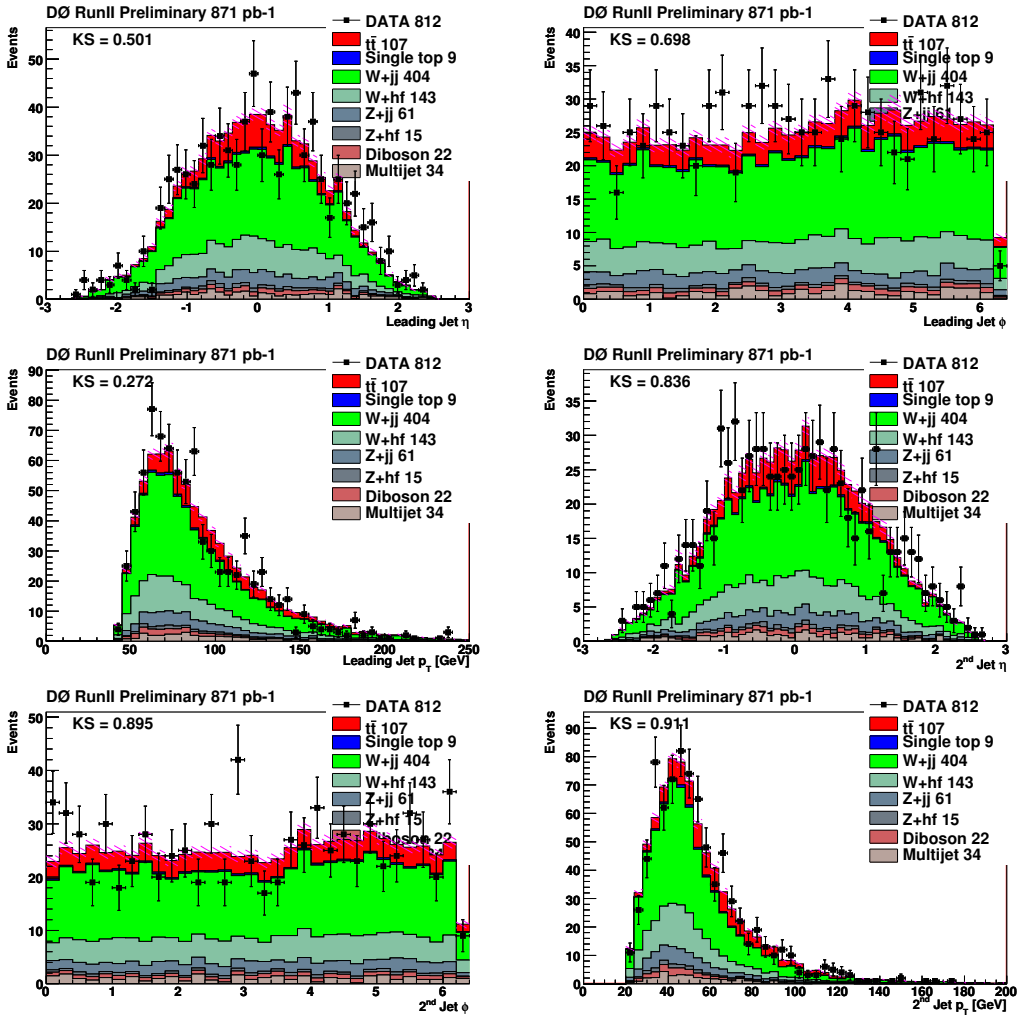

FIG. 36: *3-jet-bin* : Various distributions for the data overlaid with the result from the fit of $t\bar{t}$ (6.8 pb), backgrounds and QCD-multijets for the μ+jets analysis.

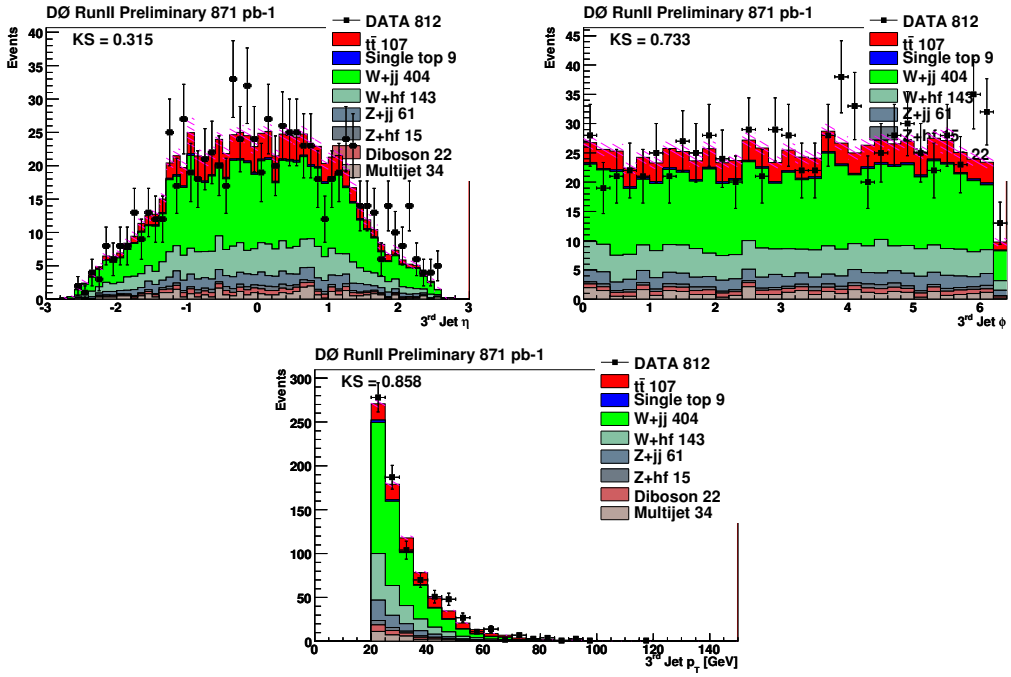

FIG. 37: *3-jet-bin* : Various distributions for the data overlaid with the result from the fit of $t\bar{t}$ (6.8 pb), backgrounds and QCD-multijets for the μ+jets analysis.

APPENDIX D: CONTROL PLOTS FOR 4 JET BIN CHANNEL

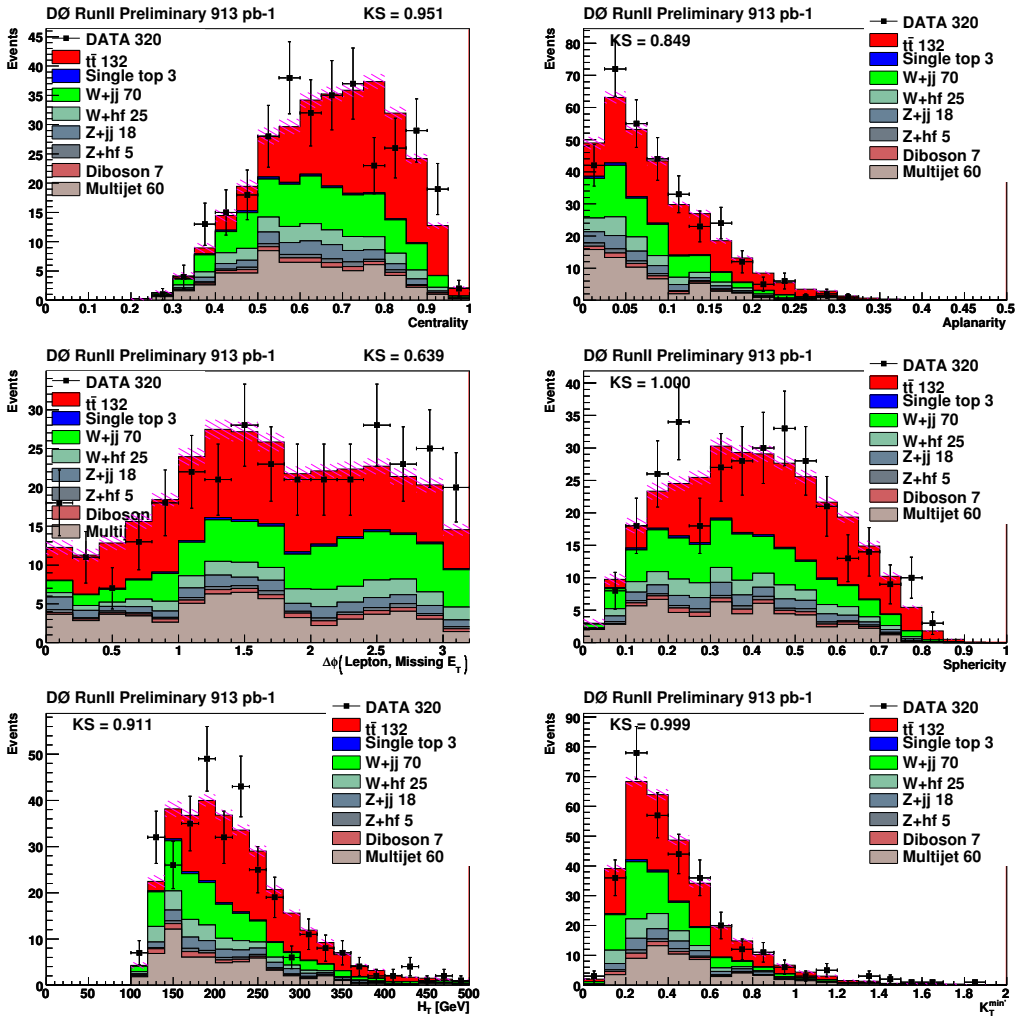

FIG. 38: *4-jet-bin* : Likelihood discriminant input distributions for the data overlaid with the result from the fit of $t\bar{t}$ (6.8 pb), backgrounds and QCD-multijets for the e+jets analysis.

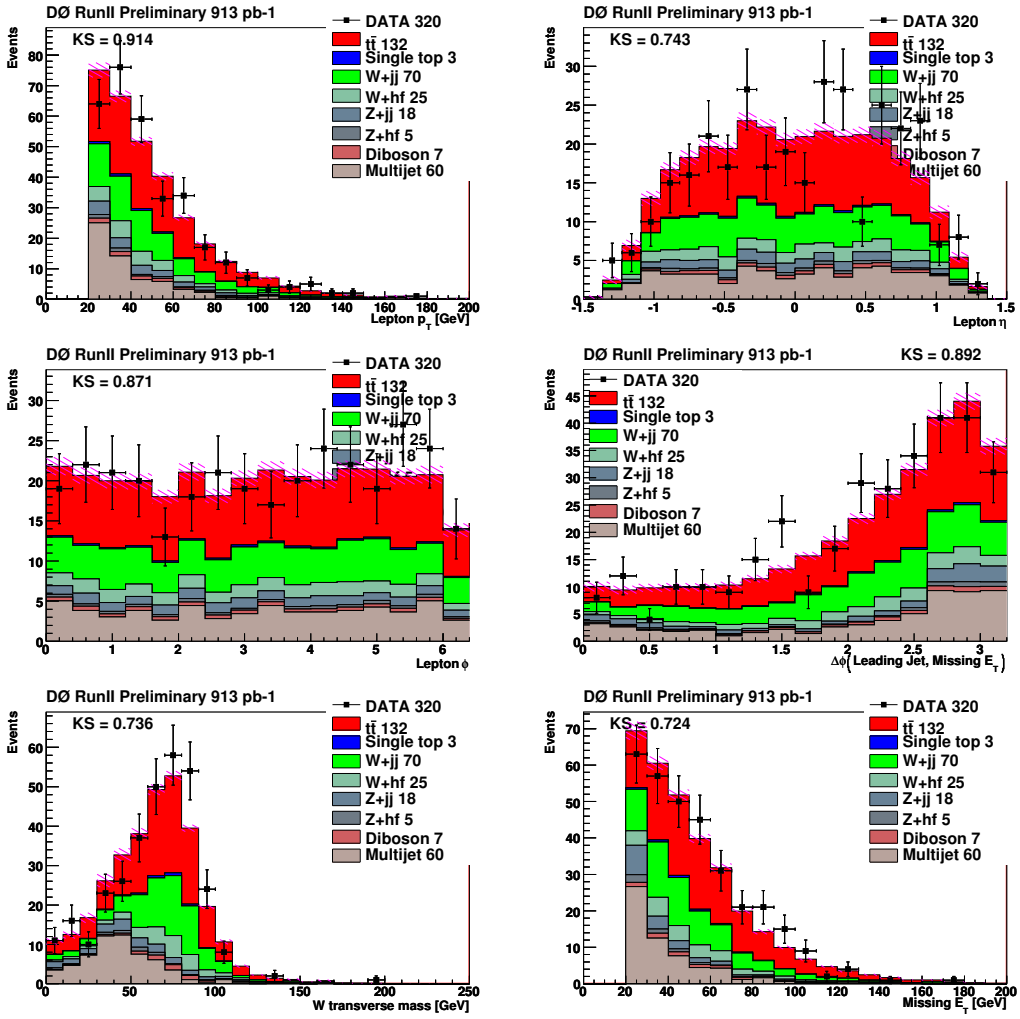

FIG. 39: *4-jet-bin* : Various distributions for the data overlaid with the result from the fit of $t\bar{t}$ (6.8 pb), backgrounds and QCD-multijets for the e+jets analysis.

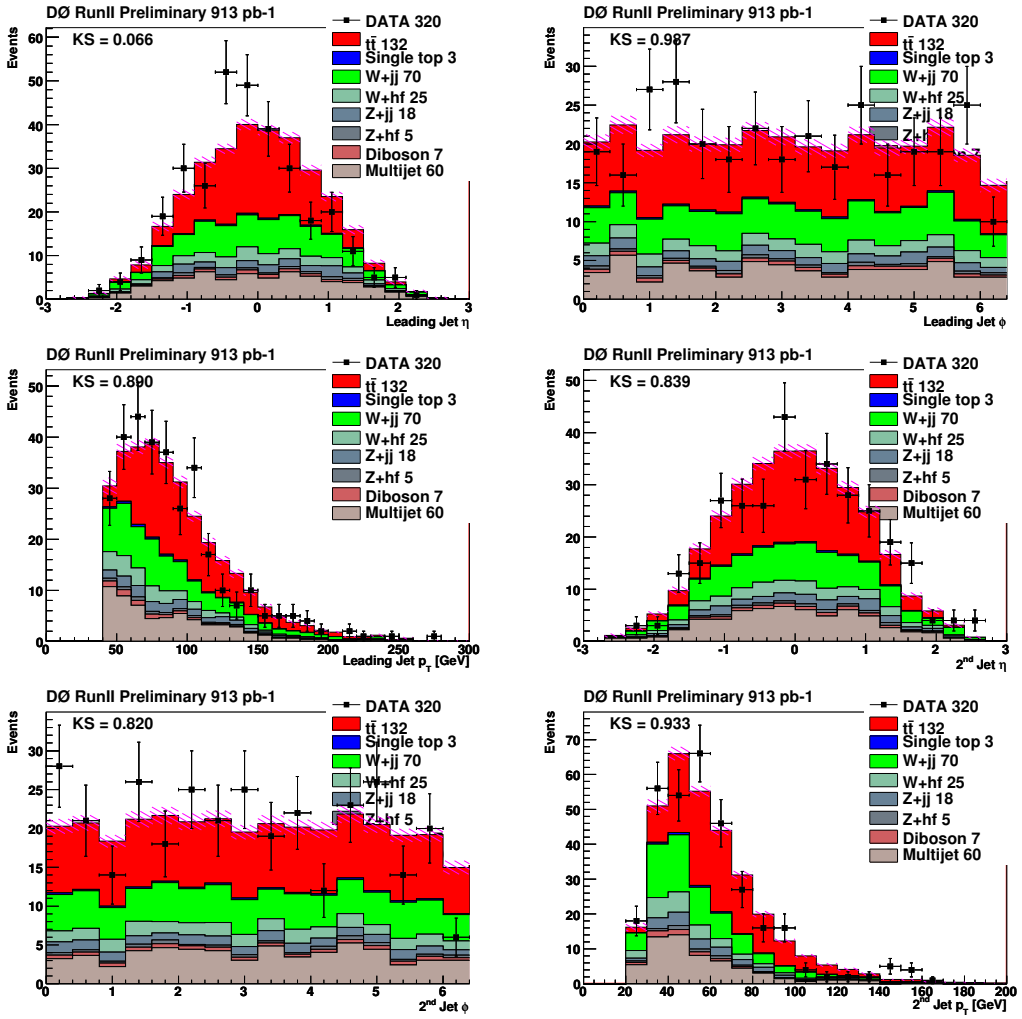

FIG. 40: *4-jet-bin* : Various distributions for the data overlaid with the result from the fit of $t\bar{t}$ (6.8 pb), backgrounds and QCD-multijets for the e+jets analysis.

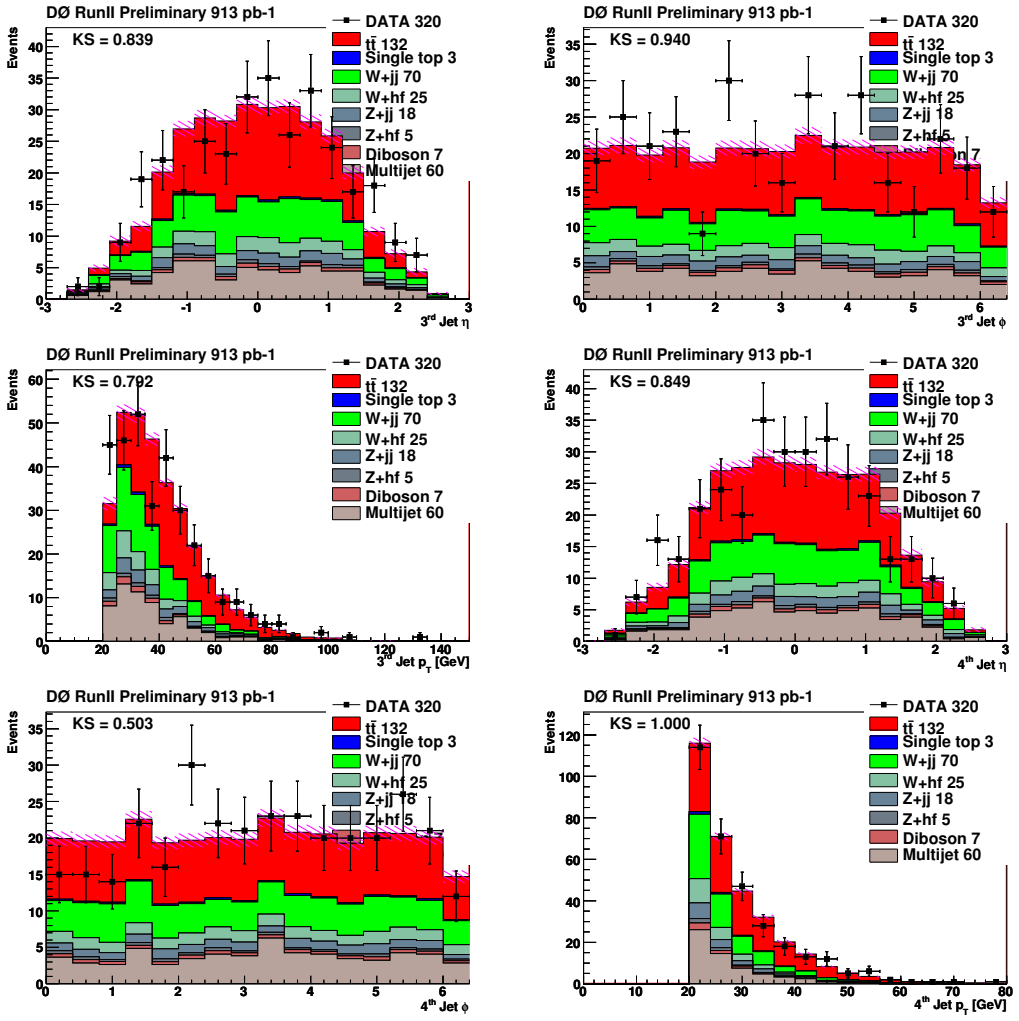

FIG. 41: *4-jet-bin* : Various distributions for the data overlaid with the result from the fit of $t\bar{t}$ (6.8 pb), backgrounds and QCD-multijets for the e+jets analysis.

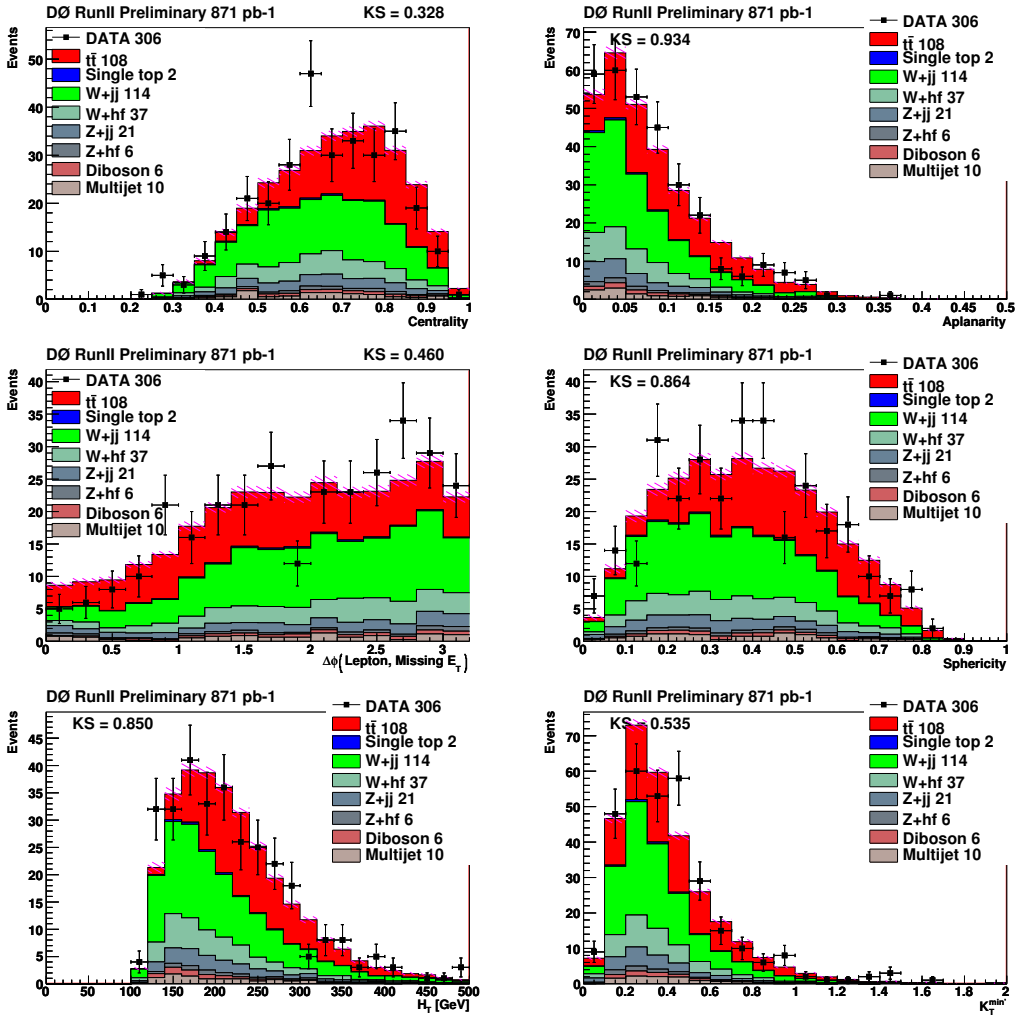

FIG. 42: *4-jet-bin* : Likelihood discriminant input distributions for the data overlaid with the result from the fit of $t\bar{t}$ (6.8 pb), backgrounds and QCD-multijets for the μ+jets analysis.

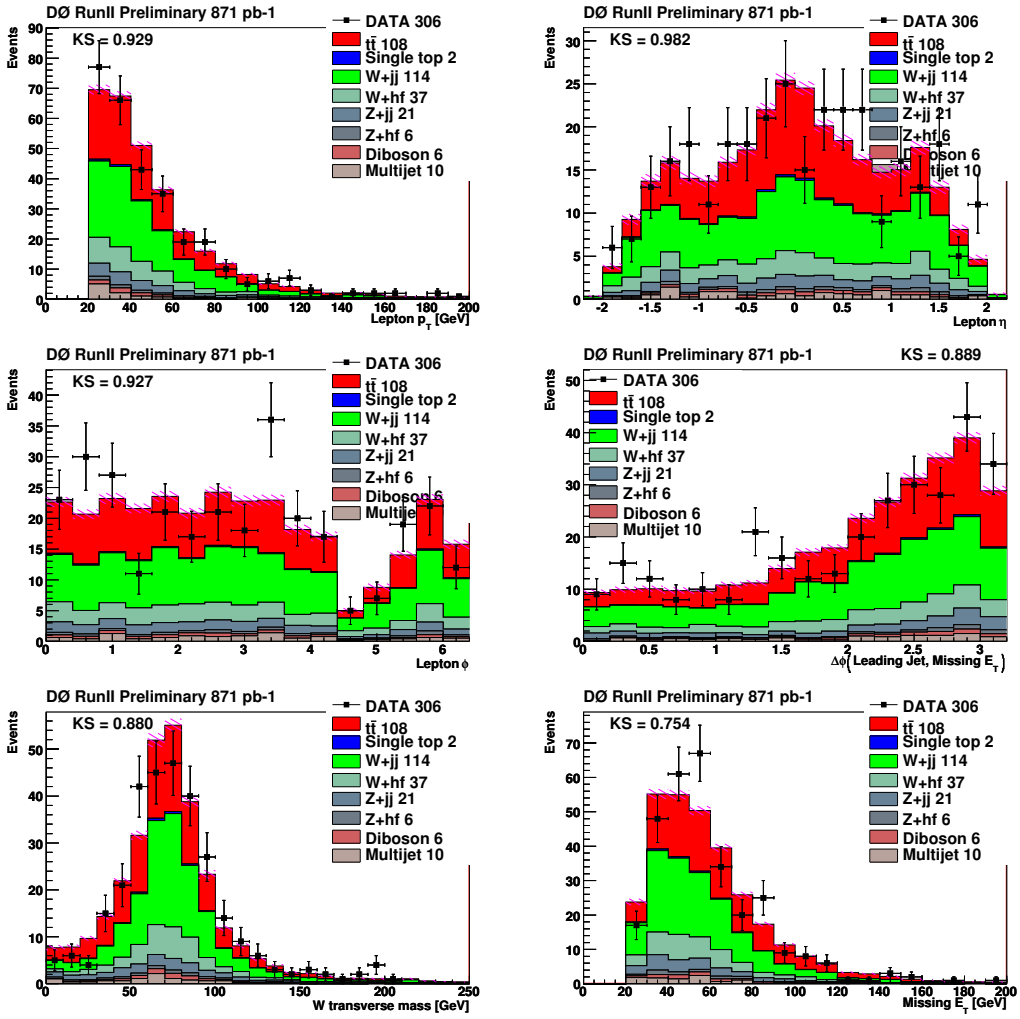

FIG. 43: *4-jet-bin* : Various distributions for the data overlaid with the result from the fit of $t\bar{t}$ (6.8 pb), backgrounds and QCD-multijets for the μ+jets analysis.

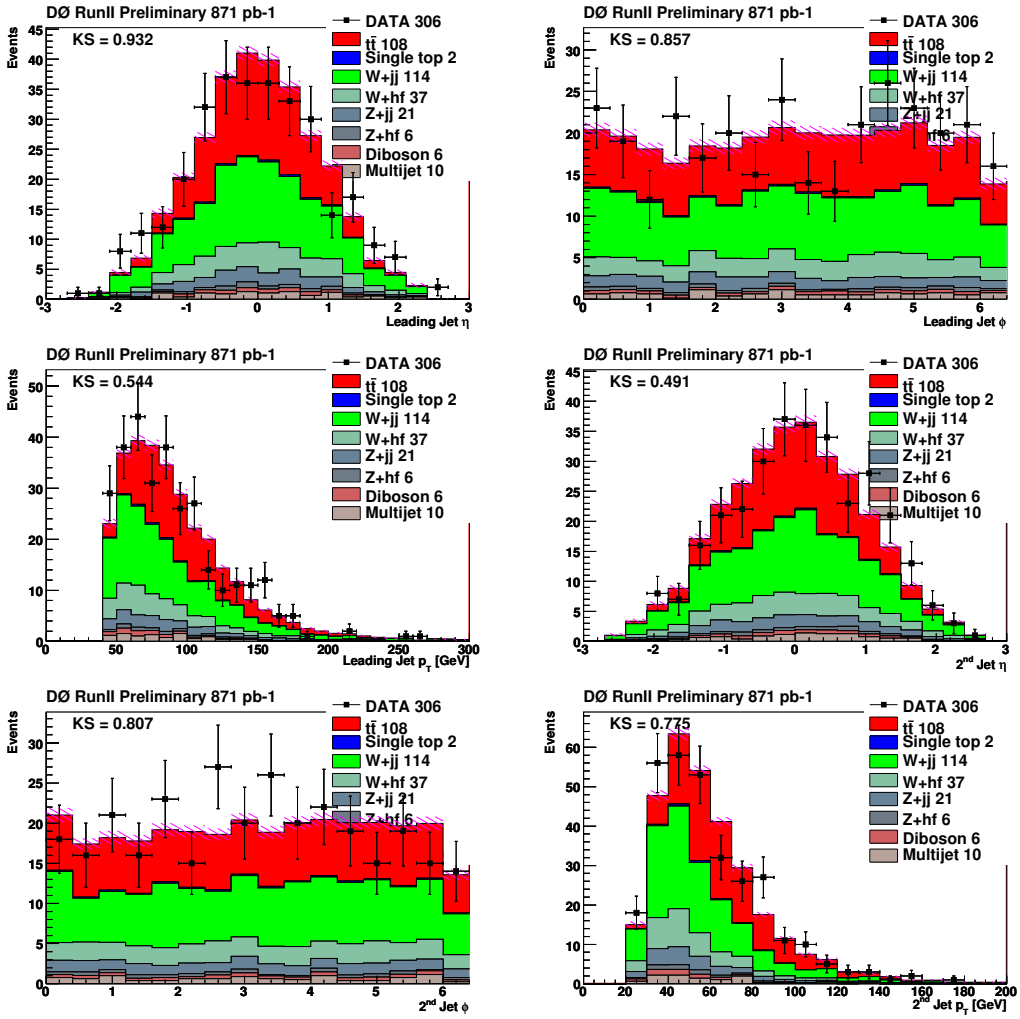

FIG. 44: *4-jet-bin* : Various distributions for the data overlaid with the result from the fit of $t\bar{t}$ (6.8 pb), backgrounds and QCD-multijets for the μ+jets analysis.

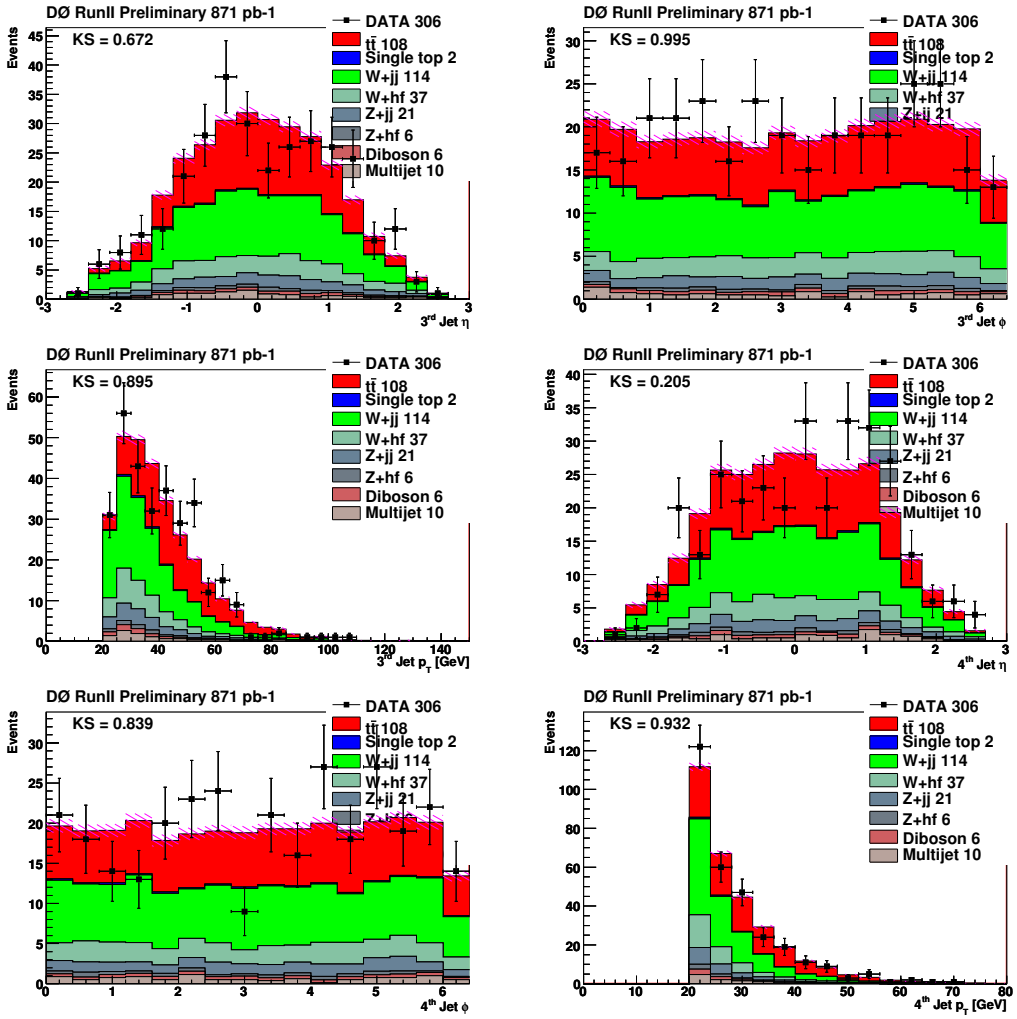

FIG. 45: *4-jet-bin* : Various distributions for the data overlaid with the result from the fit of $t\bar{t}$ (6.8 pb), backgrounds and QCD-multijets for the μ+jets analysis.

[1] N. Kidonakis and R. Vogt, Phys. Rev. D **68**, 114014 (2003).
[2] M. Cacciari, S. Frixione, G. Ridolfi, M. Mangano, P. Nason, JHEP **404**, 68 (2004).
[3] John Brunelle et al, Measurement of the $t\bar{t}$ Production Cross-Section at $\sqrt{s} = 1.96$ TeV in the Lepton+Jets Final State using a Topological Method on 1 fb^{-1} of DØData, DØNote 5249, October 2006.
[4] A. Schwartzman and C. Tully, *Primary Vertex Reconstruction by Means of Adaptive Vertex Fitting*, DØ Note 4918, September 2005.
[5] J. Hays *et al.*,"Single Electron Efficiencies in p17 Data and Monte-Carlo using p18.05.00 d0correct,"DØ Note 5105 (2006).
[6] T. Gadfort *et al.*, "Muon Identification Certification for p17 Data," DØ Note 5157 (2006).
[7] Amnon Harel *Jet ID optimization*, DØNote 4919
[8] Jets and Missing Et, `http://www-d0.fnal.gov/~d0upgrad/d0_private/software/jetid/jetid.html`.
[9] DØCertified Jet Energy Scale, `http://www-d0.fnal.gov/phys_id/jes/d0_private/certified/certified_jes.html`.
[10] A. Schwartzman, Y. Peters, H. Greenlee *Adaptive Primary Vertex Certification in p17*, DØ Note 5192, Preparation.
[11] J. Kozminski et al., The electron likelihood in p14, DØ note 4449, November 2003.
[12] G. Garzon et al, Measurement of the ttbar Production Cross Section in ppbar Collisions at sqrt(s)=1.96TeV using Secondary Vertex b-Tagging, DØNote 5113
[13] J-R. Vlimant, U. Bassler, G. Bernardi and S. Trincaz-Duvoid, Technical description of the T42 algorithm for the calorimeter noise suppression, DØ note 4146, Mai 2003.
[14] G. Blazey, et al., Run II Jet Physics, DØ note 3750, April 2000.
[15] "Preliminary p17 JES for Data and MC (JetCorr v07-01-02)," `http://www-d0.fnal.gov/phys_id/jes/d0_private/certified/certified_jes.html`.
[16] The method is described for p14 in:
N. Makovec and J.-F. Grivaz, "Shifting, Smearing and Removing Simulated Jets," DØ Note 4914 (2005).
Application of the method in p17 can be seen here:
C. Ochando, "SSR in p17," DØ p17 Higgs Workshop, May 17-18, 2006,
`http://www-d0.hef.kun.nl//fullAgenda.php?ida=a06904&fid=32`.
[17] Common Sample Group, `http://www-d0.fnal.gov/Run2Physics/cs/index.html`.
[18] 1M skims e+jets and μ+jets, `https://plone4.fnal.gov/P1/D0Wiki/top/datamc/1m`.
[19] The top_cafe Package, `http://www-d0.fnal.gov/Run2Physics/top/d0_private/wg/top_cafe/doxydoc/html`.
[20] DØTop Triggers, `http://www-d0.fnal.gov/Run2Physics/top/d0_private/wg/triggers/triggers.html`.
[21] Brendan Casey et al, *Determination of the Effective Inelastic p pbar Cross-Section for the DO Luminosity Measurement Using Upgraded Readout Electronics*, DØ Note 4958, November 2005.
[22] Gregory Snow et al, *Adjustments to the Measured Integrated Luminosity in Run IIa*, DØ Note 5139, June 2006.
[23] T. Sjöstrand, L. Lonnblad and S. Mrenna, *PYTHIA 6.2: PHYSICS AND MANUAL*, LU-TP-01-21, hep-ph/0108264 (2001).
[24] M. L. Mangano *et al.*, *ALPGEN, a Generator for Hard Multiparton Processes in Hadronic Collisions*, CERN-TH-2002-129, FTN-T-2002-06, hep-ph/0206293 (2002).
[25] S. Höche *et al.*, "Matching Parton Showers and Matrix Elements," hep-ph/0602031.
[26] Yvonne Peters et al, Study of the W+jets heavy flavor scale factor in p17, DØNote 5406, Sep. 2007.
[27] E.E. Boos *et al.*, "Method for Simulating Electroweak Top-Quark Production Events in the NLO Approximation: SingleTop Generator," Phys. Atom. Nucl. **69**, 1317 (2006).
[28] D. Stump *et al.*, *Inclusive Jet Production, Parton Distributions, and the Search for New Physics*, MSU-HEP-030303, hep-ph/0303013 (2003).
[29] D. Gillberg, "Heavy Flavour Removal and Determination of Weighting Factors for ALPGEN W+jets Monte Carlo," DØ Note 5129 (2006).
[30] p17 datamc, `https://plone4.fnal.gov/P1/D0Wiki/top/datamc`
[31] Data Quality Group web page:
`http://www-d0.fnal.gov/computing/data_quality/d0_private/forusers.html`. We have used the recommended tags: `caf_dq v02-01-01`, with `dq_defs v2006-05-04`. A new `dqdefs v2006-10-10` has been recently released to include the cable swap data, but the used tag covers our dataset.
[32] S. Park, M. Begel, *Efficiency of the Data Quality Calorimeter Flags*, DØNote 5324, January 2007.
[33] Yvonne Peters Elizaveta Shabalina, Simultaneous measurement of B(t → Wb)/B(t → Wq) and $\sigma(p\overline{p} \to t\bar{t}) \cdot$ B(t → Wb)^2 with p17 data, July 2007.
[34] Marc-André Pleier, Measurement of the Electron and Muon Fake Rates in Lepton+Jets Datasets, DØNote 5469 Oct. 2007.
[35] E. Aguiló *et al.*, Search for Single Top Quark Production in 1 fb^{-1} of Data, DØ Note 5285, November 2006.
[36] B. Martin et al., Measurement of the ttbar production cross section at sqrt(s)=1.96 TeV in the ee final state using p17 data set, DØNote 5386.
[37] Y. Arnoud et al, Measurement of the ttbar Production Cross-Section at sqrt(s)=1.96 TeV in the Dilepton Final States Using 1 fb^{-1}, DØNote 5371.
[38] Shaohua Fu, Andy Haas, A search for $ZH(\to e^+e^-b\bar{b})$ Production with the DØDetector in $p\overline{p}$ Collisions at $\sqrt{s} = 1.96$ TeV, DØNote 5275.
[39] TMVA root class, `http://root.cern.ch/root/html/TMVA.html`

[40] T. Andeen et al., FERMILAB-TM-2365.
[41] Bertrand Martin, presented in Collaboration meeting, September 24, 2007:
`http://www-d0.hef.kun.nl//askArchive.php?base=agenda&categ=a071577&id=a071577s1t9/transparencies`.
[42] Heidi Schellman, The longitudinal shape of the luminous region at DØ, DØNote 5142, June 2006.
[43] Philippe Calfayan et al, Muon Identification Certification for p17 data, DØNote 5157, Feb. 2007.
[44] Yvonne Peters et al., Reweighting of the fragmentation function for the DØMonte Carlo, DØNote 5325, January 2007.
[45] Yvonne Peters et al.,Study of Monte Carlo Factorisation scale for DØ, in praperation, January 2007.